Guo et al. Stem Cell Research & Therapy (2025) 16:447
https://doi.org/10.1186/s13287-025-04544-7

Stem Cell Research & Therapy

RESEARCH Open Access

Constraint-induced movement therapy combined with mesenchymal stem cell transplantation promotes myelination and functional recovery by inhibiting PRKCD/MEK/ERK pathway in hemiplegic cerebral palsy rats

Xiaolin Guo[1,2†], Liru Liu[1†], Jie Luo[1†], Tingting Peng Jr.[1†], You Wang[1], Shiya Huang[1], Xiaoli Zeng[3], Tingting Peng Sr.[1], Aihua Chen[3], Mengru Zhong[1], Yage Zhang[1], Kaishou Xu[1*] and Lu He[1*]

Abstract

Background The core problem of hemiplegic cerebral palsy (HCP) is upper limb motor deficits with high rates of disability. Given the shared goals of stem cell therapy and rehabilitation, this study investigated the synergistic effects of constraint-induced movement therapy (CIMT) and human umbilical cord-derived mesenchymal stem cells (hUC-MSCs) transplantation in promoting motor recovery and elucidates the underlying mechanisms in HCP.

Methods The rats were allocated to a control group and HCP groups receiving different interventions (CIMT, hUC-MSCs or combination treatment), namely, the Control, HCP, HCP + CIMT, HCP + MSC, and HCP + CIMT + MSC groups. Motor function was evaluated using rotarod duration, grip strength, and forelimb suspension time. Golgi-Cox staining, transmission electron microscopy, immunofluorescence staining, Western blotting, quantitative real-time PCR and label-free proteomic quantification technology were used to measure dendritic/axonal area, myelin integrity, oligodendrocyte (OL)/oligodendrocyte precursor cell (OPC)-associated proteins and PRKCD/MEK/ERK expression in the motor cortex.

Results Rats in the HCP + CIMT + MSC group exhibited improved motor function, increased dendritic spines and branches, enhanced myelin integrity, higher numbers of $Olig2^+$OL, $CNPase^+$OL and MBP^+OL, and reduced $NG2^+$OPC counts in the motor cortex compared to the HCP group ($p < 0.05$). Additionally, motor performance in the

†Xiaolin Guo, Liru Liu, Jie Luo and Tingting Peng Jr. Co-first authors.

*Correspondence:
Kaishou Xu
xksyi@126.com
Lu He
kittyhelu@126.com

Full list of author information is available at the end of the article

HCP + CIMT + MSC group was significantly superior to than those in the HCP + CIMT and HCP + MSC groups ($p < 0.05$). Moreover, proteomic analysis identified that PRKCD, a key mediator of the synergistic effect, was expressed in OPC and implicated in their physiological processes. Rats in the HCP + CIMT + MSC group also showed reduced PRKCD protein and mRNA expression, fewer $PRKCD^+/NG2^+$ cells, higher $CNPase^+/PRKCD^+$ area ratio and lower levels of MEK1/2 and ERK1/2 phosphorylation relative to the HCP group ($p < 0.05$).

Conclusions CIMT combined with hUC-MSCs transplantation synergistically promoted OPC differentiation into immature OL, induced myelination, and restored motor function in HCP rats, potentially by inhibiting the PRKCD/MEK/ERK pathway. This combined approach expands therapeutic options for HCP and identifies a promising target for future interventions.

Keywords Combination therapy, Constraint-induced movement therapy, Mesenchymal stem cells, Motor function, Oligodendrocyte progenitor cells differentiation, Myelination

Introduction

Cerebral palsy (CP) is a disorder of central motor and postural development caused by non-progressive injury to the developing fetal or infant brain [1], with a global prevalence of 1.6–3.4 per 1000 births worldwide [2]. Individuals with CP require lifelong rehabilitation, contributing to significant economic and social burdens worldwide [3, 4]. It is imperative to explore effective strategies that maximize the brain's developmental plasticity and incorporate evidence-based approaches [4].

Constraint-induced movement therapy (CIMT) effectively improves limb dysfunction in children with hemiplegic CP (HCP), which accounts for about 44% of CP cases [4, 5]. CIMT enhances movement quality and efficiency in the affected limb through experience-dependent neuroplasticity, which is reflected in neuron, dendrites/axon area, and myelin remodeling [6–8]. However, its effectiveness is constrained by prolonged training durations, intensive rehabilitation resource demands, and limited efficacy in severe cases [9, 10].

Stem cell therapy offers significant potential to repair brain tissue and enhance functionality in CP [11, 12], acting via paracrine effects, immunomodulation, neuroprotection, angiogenesis, and myelin regeneration [13]. Human umbilical cord-derived mesenchymal stem cells (hUC-MSCs) isolated from Wharton's jelly are particularly advantageous due to their accessibility, low immunogenicity, reduced tumorigenicity, high proliferative rate and minimal ethical concerns [14–16], with clinical studies further proving their efficacy in diverse therapeutic applications [17, 18]. Our previous findings demonstrated that intrathecal injection of hUC-MSCs from the Wharton zone induced oligodendrocyte (OL) differentiation and myelination [19]. Importantly, intracerebral transplantation of hUC-MSCs in rodent models did not elicit significant immune rejection or adverse effects, positioning hUC-MSCs transplantation as a promising CP treatment [20, 21].

Most HCP cases result from focal vascular brain injury or unilaterally restricted periventricular white matter lesions [22, 23]. These injuries are associated with disrupted cerebral white matter integrity, prolonged OL differentiation deficits, and reduced plasticity [24, 25]. Enhancing neural circuit functionality and promoting neuronal remodeling and myelination represent promising therapeutic strategies. Integrating stem cell therapy with rehabilitation could foster a supportive tissue environment and drive functional neural circuit development, facilitating brain repair and functional recovery [26, 27].

Given the shared objectives of stem cell transplantation and rehabilitation [27], combining these approaches may enhance the functional prognosis of CP. However, the therapeutic efficacy and underlying mechanisms of this combined treatment remain poorly understood. Therefore, this study evaluates whether combining CIMT with hUC-MSCs transplantation from the Wharton's jelly zone can synergistically improve motor recovery and facilitate myelination while exploring the underlying mechanisms in HCP.

Materials and methods

Animals and HCP rat model

The work has been reported in line with the ARRIVE guidelines 2.0. The study was approved by the Institutional Animal Care and Use Committee of Guangzhou Women and Children's Medical Center (Guangzhou, China) (Protocol RSDW-2023-01402). All experimental procedures were performed in accordance with the Guide for the Care and Use of Laboratory Animals by the National Research Council [28]. Sample size calculation using G*Power software (v3.1.9.7) determined that 80 rats (16 rats per group) would be required to achieve an 80% power level and a 5% significance level (two-sided) [29]. To compensate for 20% anticipated mortality and subsequent HCP screening, twelve pregnant Wistar rats purchased from SPF biotechnology company (Beijing, China) ($n = 12$, license No. SCXK (Jing) 2019-0010) and 112 pups were born in 12 litters. All experimental rats were housed in SPF-grade animal facilities and under

standard conditions with free food and water, appropriate humidity (40–70%), moderate temperature (22–25 °C) and a 12-hour light/dark cycle. Animals were housed at ≤5 rats per cage, with complete cage replacement and disinfection performed every 3 days.

Hypoxic-ischemic (HI) rats were established using the modified Rice-Vannucci method as previously described [19]. Eighty-nine randomly selected neonatal rats underwent left common carotid artery ligation under anesthesia with inhalation of isoflurane (R510-22, Ruiwode, China) (5% for induction and 1%-1.5% for operation) on postnatal day 5 (P5), followed by 3 h of hypoxia (8% oxygen and 92% nitrogen). Three rats were randomly selected for 2, 3, 4-triphenyltetrazolium chloride (TTC) staining 24 h after surgery. Three surgical rats died from excessive blood loss due to prolonged ligation surgery. On P18, four rats were randomly selected for Nissl staining to detect neurons and 79 rats were assessed for motor function via rotarod, grip strength and forelimb suspension tests. Seventy-three rats with motor impairment were included. Cerebral infarction, the alterations in neuronal integrity and motor function confirmed the successful establishment of the HCP model. Therapeutic interventions were administered to HCP rats from P21 to P35. On P49, all rats were euthanized by phenobarbitone sodium (100 mg/kg, intraperitoneally) after the final behavioral tests. The time course and animal assignment of the whole experiment are shown in Fig. 1.

Experimental design and intervention

Seventy-three HCP rats and 16 normal rats were finally selected for the study. Nine HCP rats were randomly selected for intracerebral hUC-MSCs tracking. Apart from rats in the control group ($n=16$), a randomized block allocation was taken to assign them to 4 experimental groups: HCP group ($n=16$), HCP + CIMT group ($n=16$), HCP + MSC group ($n=16$), HCP + CIMT + MSC group ($n=16$). Specifically, HCP rats were numbered sequentially, with every 4 consecutive numbers assigned to one of the 4 groups.

On P21, rats in the CIMT group had their unaffected forelimbs immobilized using soft adhesive tape for 8 h

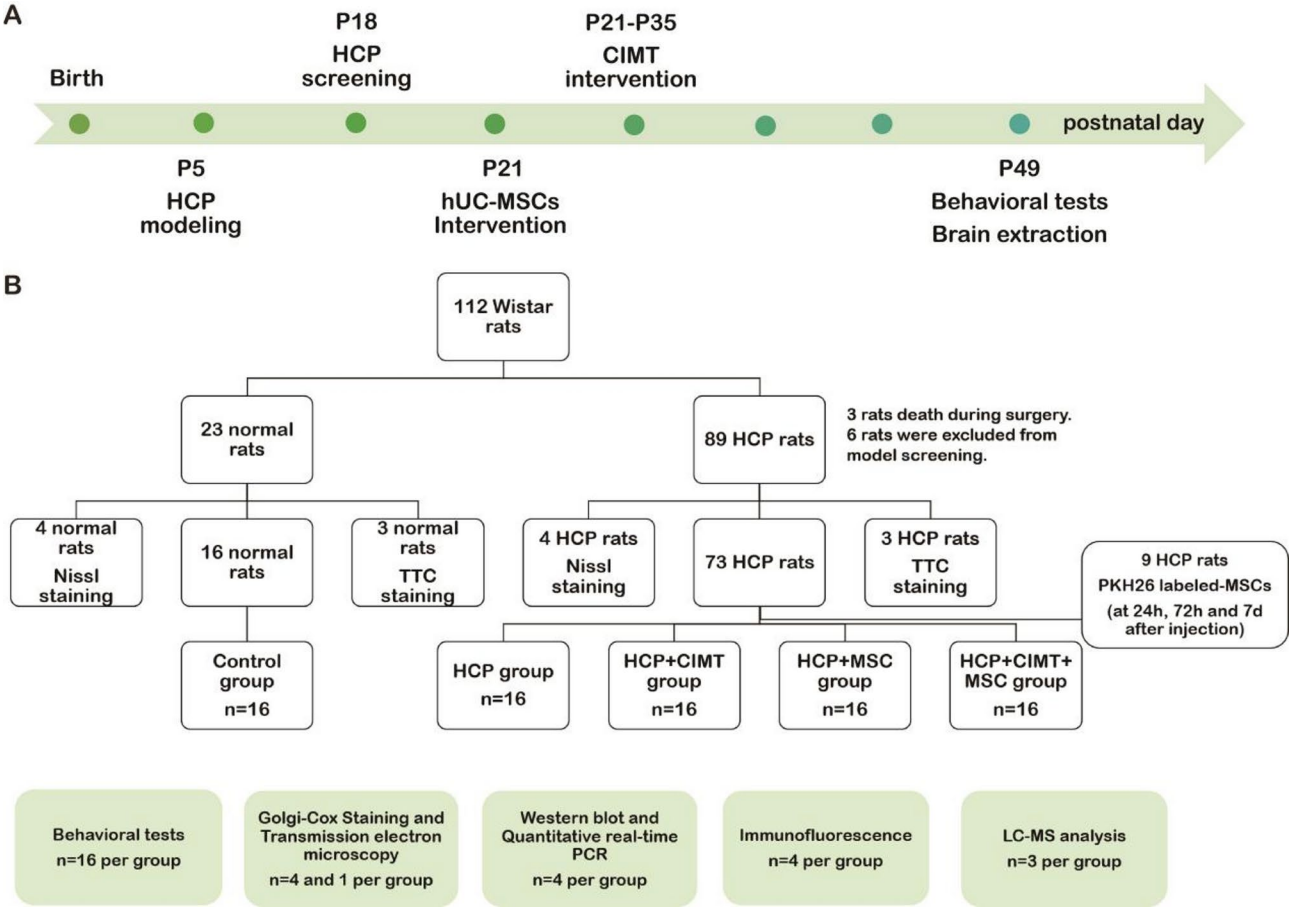

Fig. 1 The timeline and animal assignment of the whole experiment. (**A**) The timeline of this study. (**B**) Rats assignment of the whole experiment. HCP: hemiplegic cerebral palsy; CIMT: constraint-induced movement therapy; hUC-MSCs: human umbilical cord-derived mesenchymal stem cells; TTC: 2, 3, 4-triphenyltetrazolium chloride; LC-MS: liquid chromatography-mass spectrometry

daily (divided into 4-hour morning and afternoon sessions), encouraging affected forelimb (i.e. right forelimb) activity [8]. Researchers conducted continuous monitoring during restraint periods, immediately reapplying restraints if detachment occurred. They were then housed in standard cages with abundant toys and weekly-repositioned feeding and playing devices to create a novel and rich environments [30]. CIMT conducted 5 days a week for 2 weeks [8]. In the MSC group, a bolus of the cell suspension 1×10^6 hUC-MSCs in 20 µl saline was slowly intrathecally injected into each rat under anesthesia with inhalation of isoflurane (5% for induction and 1.5%-2% for operation) [19]. Prior to injection, the injection site was shaved and sterilized by povidone-iodine. The L5 spinous process was palpated with the index finger of the left hand, while the thumb and middle finger stretched the skin taut. A Hamilton syringe (20781, Hamilton, USA) was then punctured at 70–80° angle into the L5-L6 interspinous space using the right hand. Successful intrathecal injection is confirmed by the presence of tail-flicking action or hind limb twitching [31]. Post-infusion rats were placed on a heating pad (37 ± 1℃) until restoring full ambulation prior to cage return. Throughout the postoperative recovery period, all rats were continuously monitored for injection-related pain behaviors (e.g., guarding posture, vocalization). If observed, isoflurane inhalation was immediately administered for sedation and analgesia. The combination therapy group received a bolus of hUC-MSCs injection at the beginning of a two-week CIMT protocol initiated on P21. On P49, all experimental rats were humanely euthanized with sodium phenobarbital (100 mg/kg, i.p.) after behavioral assessments to harvest brain samples.

Tissue preparation

All rats were euthanized by phenobarbitone sodium (100 mg/kg, i.p.) after the behavioral tests and transcardially perfused with phosphate buffered saline (PBS) (BL601A, Biosharp, China) followed by 4% paraformaldehyde (BL539A, Biosharp, China). The brain was rapidly extracted by craniotomy. For histological examination and immunofluorescence, brain tissues were fixed by cardiac perfusion and immersion in 4% paraformaldehyde, then dehydrated and embedded according to routine sampling and fixation methods [32]. Whole brain tissues were sliced into 10-µm-thick coronal frozen sections on a microtome-cryostat (CM1860, Leica, Germany) for counting PKH26-positive cells. The motor cortical regions were sectioned into 6 µm coronal paraffin slices using a vibratome (VT1200S, Leica, Germany) for Nissl staining and immunofluorescence. For Western blot analysis and quantitative real-time PCR, the primary motor cortex (M1) of the left cerebral tissue were segmentation and then flash frozen in liquid nitrogen for subsequent experiments.

HUC-MSCs culture, identification and tracking in the brain

The hUC-MSCs used in this study were all supplied by Guangdong Xiangxue Stem Cell Regenerative Medicine Technology Co., Ltd (Guangzhou, China). The hUC-MSCs harvested from the Wharton zone in fresh umbilical cord tissue were cultured in serum-free human mesenchymal stem cell medium (G03010, Saliai, China) under a humidified atmosphere at 37 °C with 5% CO_2. When cells reached 80–90% confluence, 1.5 mL 0.25% trypsin-EDTA (25200056, ThermoFisher, USA) was added to T75 flasks and incubated for 1–2 minutes. The reaction was terminated by adding 4–5 mL of cell medium. Cells were then seeded into new T75 flasks at a density of 5.0×10^5 cells/cm^2. The culture medium was refreshed every 48–72 h, and hUC-MSCs at passages 3–5 were used for these experiments. Flow cytometric analysis was employed to analyze the stem cell phenotype. Passage 5 cells suspensions (100 µL aliquots containing 1×10^6 cells) were stained with the following fluorescence-conjugated anti-human antibodies: FITC-CD73 (344015, BioLegend, USA), APC-CY7-CD44 (103027, BioLegend, USA), FITC-CD34 (343503, BioLegend, USA), PE-CY7-CD45 (304015, BioLegend, USA). Antibody staining was performed at manufacturer-recommended concentrations (5 µL antibody per 1×10^6 cells in 100 µL volume) for 30 min at 4℃ protected from light [33]. Stained hUC-MSCs were analyzed by a NovoCyte flow cytometer (NovoCyte, Agilent, USA).

The hUC-MSCs were labeled with PKH26 fluorescent cell linker kits (MINI26-1KT, Sigma, USA) according to the manufacturer's protocol and then injected intrathecally on P21. Brain tissue was collected at 24 h, 72 h, and 7 days post injection, coronally sectioned into 10 µm slices. Transplanted cells were counted in each hemisphere in the five sections per brain corresponding to Figures 10, 20, 30, 40 and 50 of Paxino's rat brain atlas [34] using a fluorescence microscope ((DMI3000B, Leica, Germany). PKH26-positive cells with 49,69-diamidino-2-phenylindole dihy drochloride hydrate (DAPI)-positive nuclei in each hemisphere were counted using Image J software (National Institutes of Health, USA). The total number of hUC-MSCs per brain tissue was quantified by counting positively labeled cells across five representative tissue sections.

Behavioral tests

Rotarod test

The rotarod test was implemented to assess motor balance and coordination in rats. Prior to formal testing, all rats underwent 3 training sessions at 30 rpm for 5 min each. During testing, the speed of rotation was increased

uniformly from 4 rpm to 40 rpm within 5 min. The test was concluded when the rat fell off the rotarod (LE8305, Panlab, Spain). Each rat was tested 3 times and the average duration on the rotarod was recorded on P18 and P49.

Grip strength test

The forelimb grip strength in rats was measured using a grip strength tester (ZL-010, INNOTEG, China). During testing, only the forepaws of the rat was allowed to grasp the grid. As the rat grasped the grille, the experimenter pulled their tails horizontally until they completely released the grip and recorded grip. Each rat underwent tested 3 times on P18 and P49.

Front-limb suspension test

A 0.5 cm diameter horizontal wire was suspended 45 cm above the operating platform to allow forelimb grasping, and soft padding was placed underneath. The time until the rat's fall was recorded and the average of three fall durations was analyzed on P18 and P49.

TTC staining

Brain tissues of rats ($n = 3$) in the control and HCP groups were rapidly removed 24 h after surgery under anesthesia with inhalation of 5% isoflurane and then 5 consecutive 2-mm coronal slices were prepared. Brain slices were incubated in a 2% solution of TTC (G3005, Solarbio, China) at 37 °C for 30 min and immersed in 4% paraformaldehyde. The viable brain area was stained dark red, reflecting intact mitochondrial function, while the infarcted area remained unstained. The stained brain sections were photographed with a digital camera and the cerebral infarct area ratio was analyzed using Image J software [35].

Nissl staining

Brain paraffin sections from P18 in the control and HCP groups ($n = 4$) were heated at 67℃ for 1 h, then dewaxed with xylene for 40 min. Sections were immersed in anhydrous ethanol for 10 min, 95% ethanol for 5 min, 75% ethanol for 5 min and double distilled water (DDW) for 5 min. Nissl staining of the above samples was performed at 57℃ for 30 min using toluidine blue (G3663, Solarbio, China). Slides were washed with DDW until colorless. Slides were fractionated with 95% ethanol (40 s) and dehydrated in xylene (10 min). After staining, images were captured using an orthogonal microscope (DMI3000B, Leica, Germany). Three regions per section were selected for neuron counting using Image J software.

Golgi-cox staining

Brain tissues from rats in each group ($n = 4$) were directly removed and processed according to the instructions of the commercially procurable FD Rapid Golgi Stain Kit (PK401, FD Neurotechnologies, Colombia) [36]. The coronal surfaces of the motor cortex tissues embedded in agarose were then cut into 150 μm thick sections. The sections were mounted, dehydrated and sealed. Imaging was conducted using an microscope (Eclipse Ci-L, Nikon, Japan). Reconstruction of individual neurons was performed using Image-Pro Plus software (Media Cybernetics, USA). The number of dendritic spines in the 30–90 μm length range of the 2nd or 3rd dendritic branch on a single neuron was quantified. Neuronal structure was mapped using the Neuron J plug-in in Image J software. The Sholl analysis plug-in created 10 concentric circles 10 μm apart with the cytosol as the center. The number of intersections of the dendrites with the concentric circles was counted and the sum of the 10 intersections was calculated.

Transmission electron microscopy (TEM)

After inducing anesthesia, rats in each group ($n = 1$) received an intracardiac perfusion (methods as described above). Then, brain tissue samples with a 1 mm^3 segment of the motor cortex was fixed overnight at 4℃ in a phosphate solution containing 4% paraformaldehyde and 2.5% glutaraldehyde (BL910A, Biosharp, China). Following routine dehydration and embedding, tissue blocks were sectioned into 80-nm ultrathin slices using an ultramicrotome (EM-UC7, Leica, Germany), which were then stained with uranyl acetate and lead citrate. Ultrathin sections of stained tissues were examined by electron microscopy. Myelin morphology and ultrastructure of the motor cortex pyramidal cell layer were observed using a 135,000× TEM (H-7500, Hitachi, Japan) [37].

Western blot analysis

Frozen cortical tissues from each group of rats ($n = 4$) were homogenized in 200 μL radio immunoprecipitation assay (RIPA) buffer (P0013B, Beyotime, China) supplemented with 2 μL phenylmethylsulfonyl fluoride (PMSF) (ST506, Beyotime, China) and 2 μL phosphatase inhibitor (P1045, Beyotime, China) and then completely lysed using a pre-chilled tissue grinder (KZ-II, Servicebio, China). The protein concentration of each sample was adjusted to 5 μg/μL using a BCA kit (PC0020, Solarbio, China). Equal amounts (30 μg) of proteins were separated by sodium dodecyl-polyacrylamide gel electrophoresis (6%-12.5%) (PG112, EpiZyme, China) and transferred to a polyvinylidene fluoride (ISEQ00010, Millipore, USA). The membrane was then incubated with primary antibodies against rabbit antibody to neuron-glial antigen 2 (NG2) (Abcam, ab129051, 1:1000), rabbit antibody to 2',3'-cyclic

nucleotide 3'-phosphodiesterase (CNPase) (Cell Signaling Technology, 5664S, 1:1000), rabbit antibody to myelin basic protein (MBP) (Cell Signaling Technology, 78896S, 1: 1000), rabbit antibody to oligodendrocyte transcription factor 2 (Olig2) (Abcam, ab109186, 1:1000), rabbit anti-protein kinase C delta (PRKCD) (Abcam, ab182126, 1:1000), rabbit anti-p-MEK1/2 (Cell Signaling Technology, 9154T, 1:1000), rabbit anti-p-ERK1/2 (Cell Signaling Technology, 4370T, 1:1000). Membranes were then incubated with Goat Anti-Rabbit IgG H&L (HRP) secondary antibodies (Abcam, ab6721, 1:2000) at room temperature for 1 h. The protein bands were detected by Enhanced chemiluminescence imaging system (Alliance Q9, UVITEC, UK). Mouse anti-HSP90 (Proteintech, 60318, 1:2000) and rabbit anti-β-tubulin (Affinity, AF7011, 1:2000) were served as internal reference for quantitative measurement of protein expression levels. Densitometric and quantitative analysis of protein bands was performed using Image J software [38].

Immunofluorescence

Brain paraffin sections from each group ($n = 4$) were heated at 67℃ for 1 h, then dewaxed with xylene for 40 min. Sections were sequentially soaked in anhydrous ethanol for 10 min, 95% ethanol for 5 min, 75% ethanol for 5 min and DDW for 15 min. Sections were performed antigen repair with 20× citrate antigen retrieval buffer (G1202, Servicebio, China) and permeabilized with 0.5% Triton X-100 (ES-8090, EcoTopBio, China) for 15 min at room temperature. Sections were blocked with 10% fetal bovine serum for 1 h at room temperature and then incubated overnight at 4℃ with primary antibodies rabbit anti-NG2 (Abcam, ab129051, 1:200), rabbit anti-CNPase (Cell Signaling Technology, 5664S, 1: 200), rabbit anti-MBP (Cell Signaling Technology, 78896S, 1:50), rabbit anti-Olig2 (Abcam, ab109186, 1:150), rabbit anti-PRKCD (Abcam, ab182126, 1:200). The sections were then exposed to goat anti-rabbit antiserum (Alexa Fluor 594/488, Abcam, ab150080, 1:200) for 1 h at room temperature in the dark. The slides were incubated with DAPI solution (MBD0015, Sigma-Aldrich, Germany) for 8 min and then sealed with the anti-quenching fluorescent. Fluorescence images were captured using a fluorescence microscope (DMI3000B, Leica, Germany) and image data were analyzed using Image J software [39].

Quantitative real-time polymerase chain reaction (qPCR)

Total RNA was extracted using TRIzol reagent (15596018CN, Invitrogen, USA) according to the manufacturer's instructions. Complementary DNA (cDNA) production and Q-PCR were performed by using RT First Strand Kit (K1671, Servicebio, China) and SYBR Green qPCR Master Mix (G3323, Servicebio, China). The primer sequences were as follows: PRKCD, forward, 5'ACCTCTTCTTTGTGATGGAGTTCC3', reverse, 5'AGCTTGAGGTCCCTGTAAATGATG3'; β-actin, forward, 5'AGCCATGTACGTAGCCATCCA3', reverse, 5'TCTCCGGAGTCCATCACAATG3'. PCR was performed in triplicate using a real-time PCR detection system (CFX96, Biorad, USA) and the threshold cycle numbers of each sample were averaged, and the relative fold change in PRKCD expression was compared using the $2^{-\Delta\Delta CT}$ method [40].

Liquid chromatography-mass spectrometry (LC-MS) analysis

Briefly, brain tissue samples ($n = 3$) were lysed and quantified by BCA assay. The samples were then sequentially subjected to acetone precipitation, tryptic digestion, sodium deoxycholate cleanup, and peptide desalting. For each sample, nearly 2 μg of peptide was separated and analyzed using nano-UPLC (EASY-nLC1200, Thermo Scientific, USA) coupled to mass spectrometry (Q Exactive, Thermo Scientific, USA). Separation was performed using a reversed-phase column (100 μm, ID×15 cm, Reprosil-Pur 120C18-AQ, 1.9 μm, Dr. Math). Data dependent acquisition was performed in profile and positive mode with Orbitrap analyzer at a resolution of 70,000 (@200 m/z) and m/z range of 350–1600 for MS1. For MS2, the resolution was set to 17,500 with a dynamic first mass. The automatic gain control target for MS1 was set to 3.0 E + 6 with max IT 50ms, and 5.0 E + 4 for MS2 with max IT 100ms. The top 20 most intense ions were fragmented by high energy collision dissociation with normalized collision energy of 27%, and isolation window of 2 m/z. The dynamic exclusion time window was 30 s.

Bioinformatics analysis

The protein sequence database (Uniprot_organism_2016_09) was downloaded from UNIPROT. This database and its reverse decoy were then searched against by MaxQuant software (Cox Lab, Germany). The quantification type was label-free quantification with match between run and intensity-based absolute quantification. Trypsin was set as specific enzyme with up to 3 miss cleavage. Oxidation (M) and Acetyl (protein N-term) were considered as variable modification (max number of modifications per peptide is 3), and Carbamidomethyl (C) was set as fixed modification. False discovery rate for peptide and protein should be less than 0.01. The screening thresholds for differentially expressed proteins (DEPs) were a fold-change more than 1.5 and a p-value less than 0.05, which was widely used in previous study [41].

Statistical analysis

Statistical analysis was performed using SPSS version 25.0 (IBM, USA) and plotted using Prism 8.0.1 (GraphPad, USA). The Shapiro-Wilk test was used to assess the

normality of the data. Comparisons between groups were made using analysis of variance (ANOVA) or non-parametric rank-sum tests. For parametric data, ANOVA followed by the least significant difference (LSD) post hoc test was used, and for non-parametric data, the Kruskal-Wallis test followed by the Bonferroni test was used as a post hoc analysis. In addition, the analysis and experimental group allocation were performed by an individual who was not involved in the experiments and assessments were conducted by evaluators blinded to group assignments. Results are presented as mean ± standard error of the mean (SEM). Statistical significance was considered when $p < 0.05$.

Results

Identification of hUC-MSCs in vitro and distribution in brain tissue of HCP rats through the intrathecal route

The cultured hUC-MSCs grew adherently to the wall. The cells were long, spindle-shaped with smooth cell wall edges (Fig. 2A). After three passages, the cell surface markers of hUC-MSCs were detected by flow cytometry. The results showed that the MSC markers CD44 and CD73 were positively expressed, whereas the hematopoietic lineage markers CD45 and CD34 were negatively expressed, indicating that the cells were typically growing hUC-MSCs (Fig. 2B). HUC-MSCs were stained with the red fluorescent marker PKH26, and the cell morphology was similar to that of unlabeled cells, with a labelling rate of approximately 100% (Fig. 2C). In the third generation of hUC-MSCs stained with PKH26, fluorescence was still detectable even after two passages (Fig. 2D-E).

We investigated the ability of hUC-MSCs migrate to brain injured areas by intrathecally transplanting PKH26-labelled hUC-MSCs. Twenty-four hours after transplantation, a large number of PKH26-labelled hUC-MSCs were observed in the cerebral cortex of the ipsilateral hemisphere (i.e. left hemisphere) and in the corpus callosum (ipsilesion vs. contralesion: $p < 0.001$, Fig. 2F-H). A small number of PKH26-positive cells were also found in the cerebral cortex of the contralateral hemisphere, but none were found in the corpus callosum, hippocampus or thalamus (Fig. 2F and G). After 72 h, PKH26-positive cells were predominantly located in the cerebral cortex and corpus callosum of the hypoxic-ischemic side, although their number had decreased (ipsilesion vs. contralesion: $p < 0.001$, 72 h vs. 24 h: $p < 0.01$, Fig. 2H). In addition, a small number of hUC-MSCs were detected 7 days after transplantation in the cerebral cortex (ipsilesion vs. contralesion: $p < 0.001$, 7d vs. 24 h: $p < 0.001$, Fig. 2H). These results suggest that hUC-MSCs could engraft in the brain via the intrathecal pathway and migrate to lesion sites.

Pathological changes and motor dysfunction occurred after hypoxia-ischemia and HCP rat model was successfully established

To simulate brain white matter injury, we used 5-day-old pups for hypoxia-ischemic. TTC staining was performed 24 h after surgery. The results showed that normal rats exhibited no infarct areas and clear intracerebral structures. In contrast, the HCP rats showed obvious infarct lesions concentrated in the cerebral cortex, with infarct areas ranging from 20 to 30% ($p < 0.001$, Fig. 3A). Thirteen days after surgery, the brain appearance of HCP rats was bilaterally asymmetric compared to normal rats, with the left hemisphere showing significant tissue atrophy (Fig. 3B). The results of Nissl staining showed that neurons in the motor cortex of normal rats were neatly arranged, with clearly Nissl bodies in the cytoplasm. In contrast, the neurons in the HCP group were sparsely and irregularly arranged, some Nissl bodies were reduced or even absent, and the number of neurons was significantly decreased ($p < 0.001$, Fig. 3C). Behaviorally, HCP rats showed a significant decrease in rotarod duration, forelimb grip strength and suspension time compared to normal rats ($p < 0.001$, respectively, Fig. 3D-F). In conclusion, HI could induce pathological injury and motor dysfunction, and the HCP rat model had been successfully established.

Combination therapy of CIMT and hUC-MSCs transplantation synergistically promoted motor recovery in HCP rats

To assess the recovery of motor function in 49-day-old rats after CIMT, MSC and CIMT + MSC interventions, we measured rotarod duration, grip strength and forelimb suspension time (Fig. 4A-C). The results indicated that rotarod duration was significantly longer in the CIMT + MSC, MSC, and CIMT groups than in the HCP group ($p < 0.05$, respectively, Fig. 4D). Notably, the CIMT + MSC group performed better than both the MSC and CIMT groups ($p < 0.05$, respectively, Fig. 4D). Grip strength and forelimb suspension time tests can be used to visualize differences in forelimb function in rats. Grip strength was significantly higher in the CIMT + MSC and MSC groups than in the HCP group ($p < 0.05$, respectively, Fig. 3E). However, no significant difference was found between the CIMT group and the HCP group, although the CIMT group was significantly lower than the CIMT + MSC group ($p < 0.01$, Fig. 4E). In addition, forelimb suspension time was significantly longer in the CIMT + MSC, MSC, and CIMT groups compared to the HCP group ($p < 0.05$, respectively, Fig. 4F). In summary, the combination of CIMT and hUC-MSCs in HCP rats promoted better recovery of motor function compared to either treatment alone, suggesting a synergistic therapeutic effect.

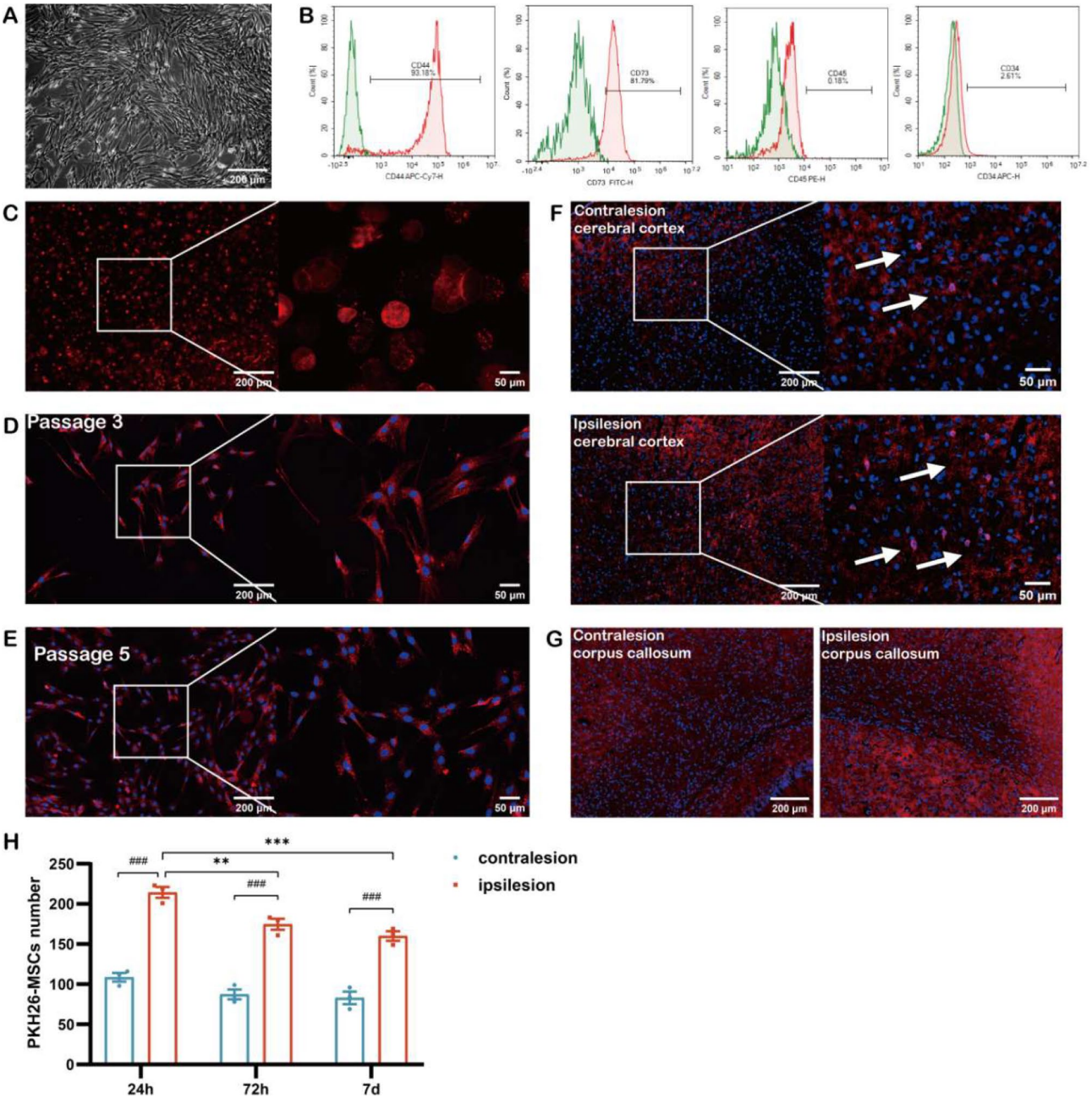

Fig. 2 HUC-MSCs morphology, identification, and distribution in the brain. (**A**) Cell morphology in PH mode of an inverted microscope, scale bar = 200 μm; (**B**) Flow cytometry of stem cell surface markers CD44, CD73, CD45, and CD34; (**C**) Immediate fluorescence after digestion of PKH26-labelled 3rd generation hUC-MSCs; (**D**) PKH26-labelled 3rd generation hUC-MSCs after cultivation for 48 h; (**E**) PKH26-labelled hUC-MSCs after 2 passages; (**F**) PKH26-labelled hUC-MSCs were distributed in the cerebral cortex and (**G**) corpus callosum, scale bar = 200 μm; (**H**) The number of surviving hUC-MSCs in the contralesion and ipsilesion at 24 h, 72 h and 7d post-injection ($n = 3$). The data are shown as the mean ± SEM. hUC-MSCs: human umbilical cord-derived mesenchymal stem cells. (** $p < 0.01$, *** $p < 0.001$ vs. 24 h; ### $p < 0.001$ vs. ipsilesion)

Combination therapy promoted dendrite and axon remodeling in the motor cortex of HCP rats

To observe the regeneration of neuronal dendrites and axons, we quantified dendritic spine density and neuronal complexity in the motor cortex based on single neuron reconstruction (Fig. 5A). The results showed that dendritic spine density was significantly greater in the CIMT + MSC, MSC, and CIMT groups compared to the HCP group ($p < 0.05$, respectively, Fig. 5B-C). We used two-dimensional Sholl analysis to graphically represent the total number of intersections is 10 concentric circles with a distance of 10 μm around soma. The results showed a significantly higher number of intersections in the CIMT + MSC group compared to the HCP group

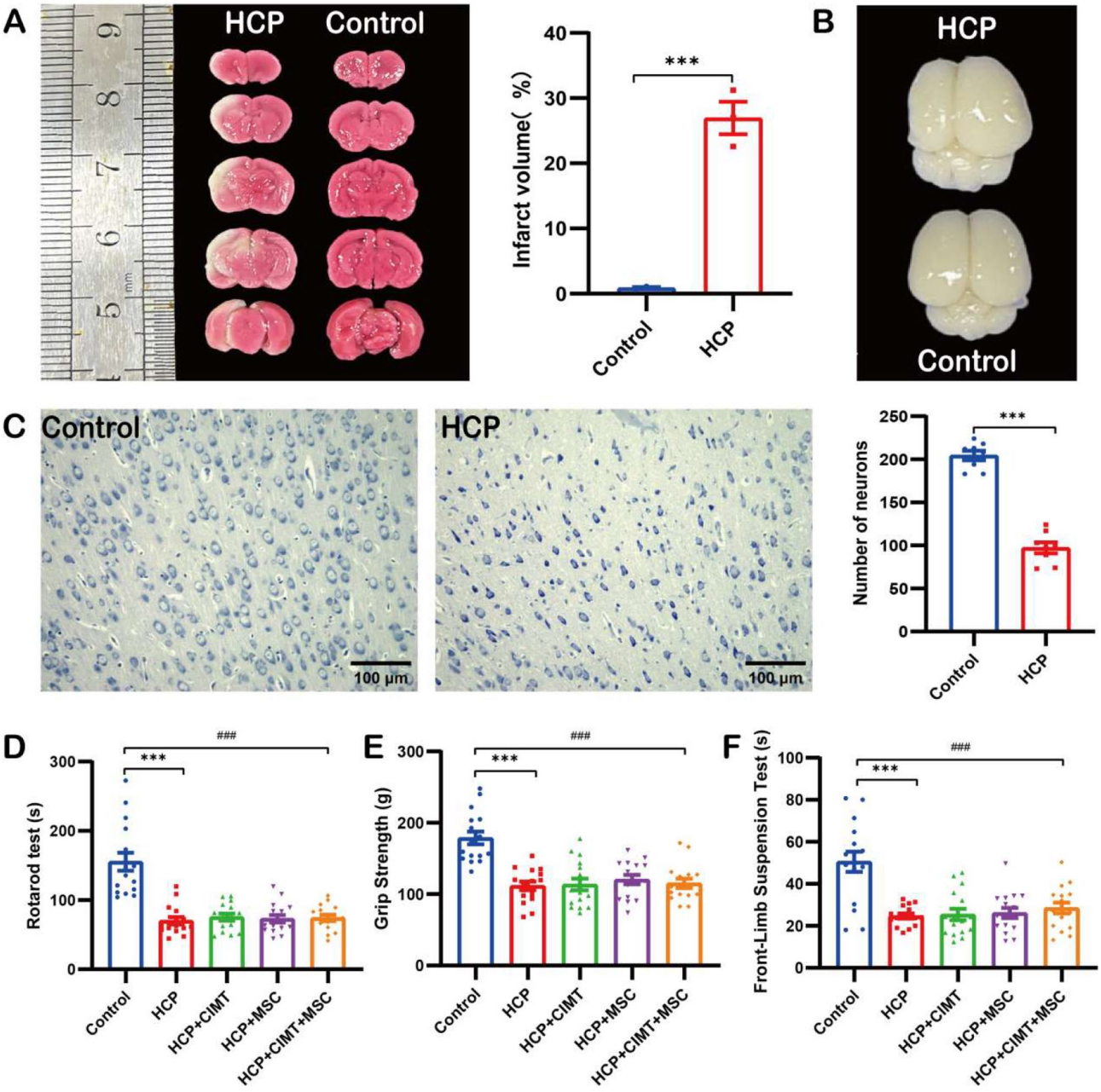

Fig. 3 Identification and screening of HCP rat models. (**A**) TTC staining at 24 h after surgery and quantitative analysis of the percentage of cerebral ischemic infarct area ($n=3$); (**B**) Brain appearance of P18 rats in control and HCP groups; (**C**) The motor cortex neurons after Nissl staining and the number of neurons analysis ($n=4*2$, 2 sections from each rat), scale bar = 100 μm; (**D**) Comparison of duration on the rotarod, (**E**) forelimb grip strength and (**F**) forelimb suspension time of rats in each group ($n=16$). The data are shown as the mean ± SEM. HCP: hemiplegic cerebral palsy; CIMT: constraint-induced movement therapy; MSC: mesenchymal stem cell; TTC: 2, 3, 4-triphenyltetrazolium chloride. (*** $p<0.001$ vs. HCP group; ### $p<0.001$ vs. HCP + CIMT + MSC group)

($p<0.01$, Fig. 5D-E). However, no statistically significant differences were observed between the CIMT, MSC, and HCP groups ($p>0.05$, Fig. 5E). Overall, the findings indicated that the combined therapy could synergistically enhance dendrite and axon remodeling.

Combination therapy enhanced OL differentiation and myelination in the motor cortex of HCP rats

We performed qualitative and quantitative analyses of oligodendrocyte precursor cells (OPC) marker NG2, immature OL marker CNPase, mature OL marker MBP, and OL transcription factor Olig2 during OL differentiation to assess myelination in the motor cortex in each

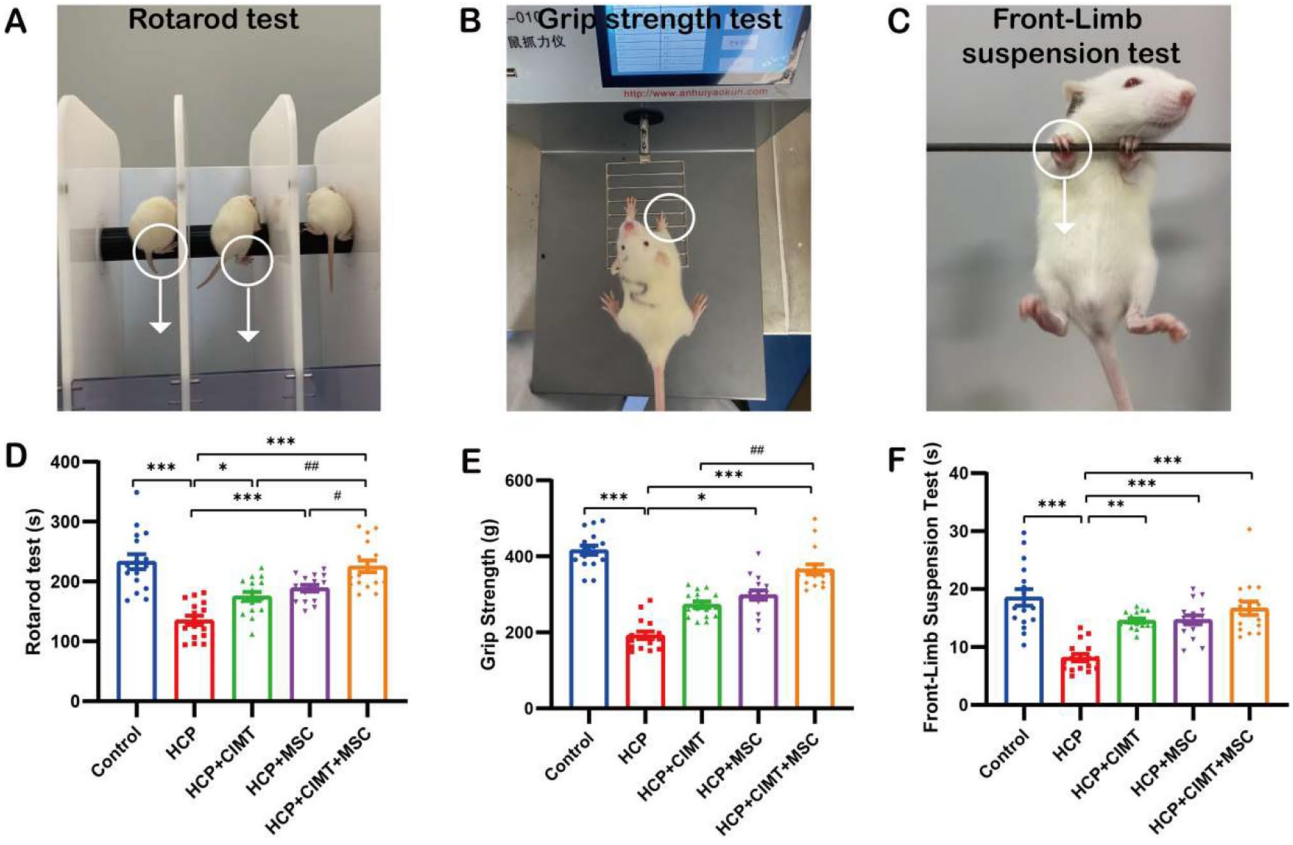

Fig. 4 Behavioral test results of rats between different groups. (**A**) Rotarod test (white arrows indicate rats dropped onto the rotarod); (**B**) Forelimb grip strength test (white circle indicates the right forelimb grip of the rat); (**C**) Front-limb suspension test (white circle indicates the right forelimb grasping of the rat and white arrows indicate rats dropped); (**D**) Comparisons of the duration on the rotarod in each group ($n = 16$); (**E**) Comparison of the forelimb grip strength in each group ($n = 16$); (**F**) Comparisons of the front-limb suspension time in each group ($n = 16$). The data are shown as the mean ± SEM. HCP: hemiplegic cerebral palsy; CIMT: constraint-induced movement therapy; MSC: mesenchymal stem cell. (* $p < 0.05$, ** $p < 0.01$, *** $p < 0.001$ vs. HCP group; # $p < 0.05$, ## $p < 0.01$, ### $p < 0.001$ vs. HCP + CIMT + MSC group)

group (Fig. 6A-B). Immunofluorescence results showed that the number of NG2$^+$ OPC was significantly higher in the HCP group compared to the control group ($p < 0.01$, Fig. 6A). The number of NG2$^+$ OPC was significantly lower after CIMT + MSC intervention ($p < 0.05$, Fig. 6A), and there was no significant effect of CIMT or MSC intervention alone on OPC activity ($p > 0.05$, Fig. 6A). The number of CNPase$^+$ OL, MBP$^+$ OL, and Olig2$^+$ OL was significantly reduced in the HCP group compared to the control group ($p < 0.05$, respectively, Fig. 6A), whereas it was significantly higher in the CIMT + MSC group than in the HCP group ($p < 0.05$, respectively, Fig. 6A). Additionally, western blot analysis of the NG2, CNPase, MBP, and Olig2 proteins further confirmed the above results (Fig. 6B).

The morphology of the myelin sheaths in the outer layer of the axons was examined by TEM to visually compare myelin regeneration (Fig. 5F). In the control group, the myelin sheaths were well organized with clear boundaries. However, in the HCP group, myelin damage was most severe, characterized by loose myelin sheaths, poor continuity and a significant reduction in myelin sheath thickness. After treatment with CIMT or MSC alone, there was a marked improvement in the arrangement and continuity of the myelin sheaths. The most significant myelination occurred in the CIMT + MSC group, which showed regular arrangement of myelin sheaths, improved continuity, and significant thickening of the myelin sheaths.

Overall, our findings suggested a massive accumulation of OPC and blocked differentiation to OL after hypoxic-ischemic brain injury in HCP rats. The combined treatment appeared to promote OL differentiation and myelination more effectively than either individual treatment alone.

Combination therapy enhanced differentiation of OPC to OL in the motor cortex of HCP rats

Protein expression levels in oligodendrocyte lineage changed significantly after the combined intervention. To further investigate the impact of the combined intervention on OL differentiation, double fluorescence

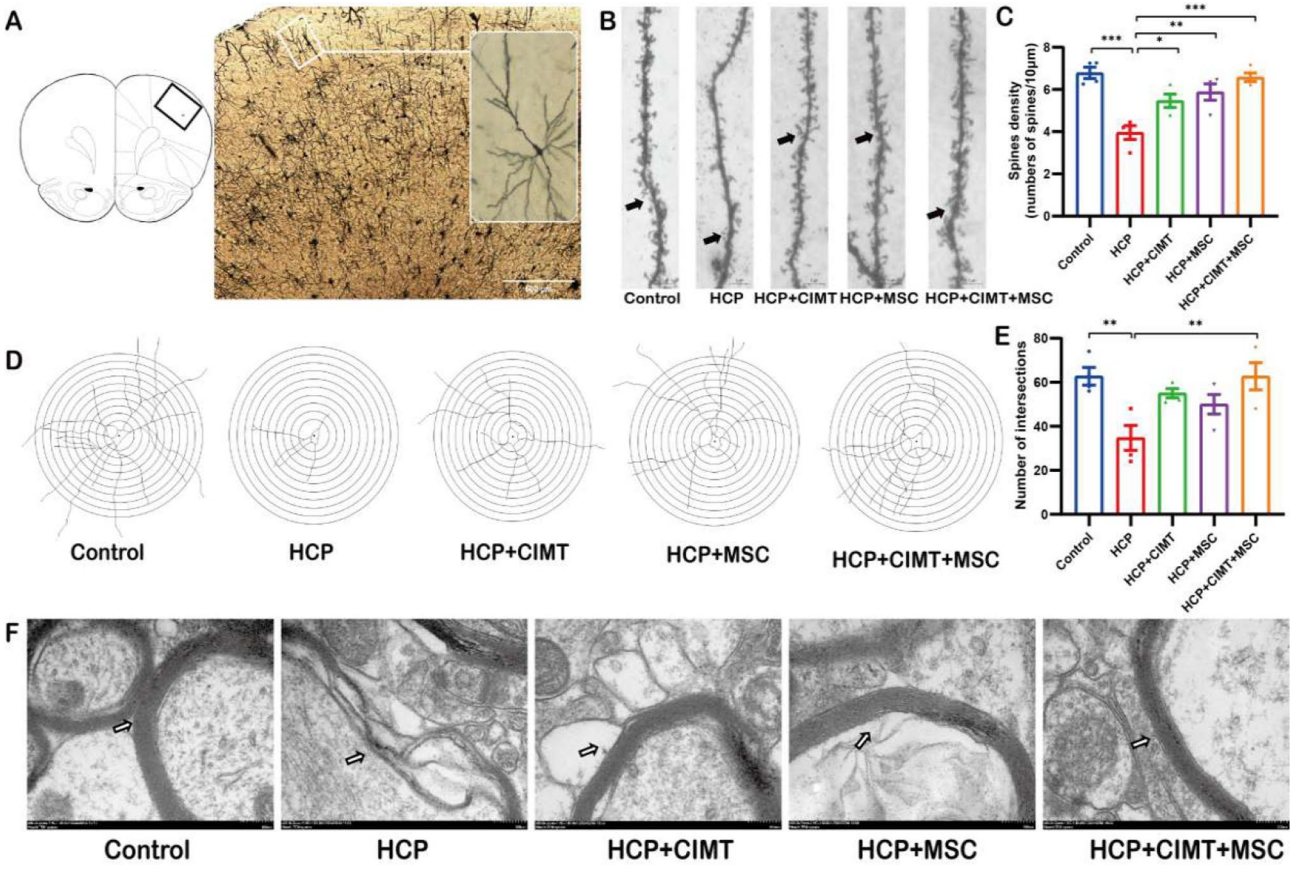

Fig. 5 The dendrite/axon remodeling and myelin ultrastructure in the motor cortex. (**A**) Neurons in the pyramidal cell layer of the motor cortex of normal rats under Golgi staining (the black box is the area of pyramidal cell layer); (**B**) Dendritic spine morphology of the motor cortex in each group, scale bar = 5 μm; (**C**) Comparison of the density of dendritic spines in each group ($n = 4$), the number of dendritic spines per 10 μm as their density = number of dendritic spines/dendritic length*10; (**D**) Reconstruction of individual neurons in the motor cortex in each group; (**E**) Total number of intersections of individual neurons with concentric circles in each group ($n = 4$), the total number of intersections is 10 concentric circles with a distance of 10 μm around soma; (**F**) Myelin ultrastructure in the motor cortex in each group, scale bar = 200 nm. The data are shown as the mean ± SEM. HCP: hemiplegic cerebral palsy; CIMT: constraint-induced movement therapy; MSC: mesenchymal stem cell. (* $p < 0.05$, ** $p < 0.01$, *** $p < 0.001$ vs. HCP group)

staining was performed for $NG2^+$ OPC and $CNPase^+$ OL (Fig. 7A). The results showed that the $NG2^+$ OPC and $CNPase^+$ OL area ratio was significantly higher in the HCP group compared to the control group ($p < 0.001$, Fig. 7A). Following the combined intervention, the NG2 area decreased while the CNPase area increased ($p < 0.001$, Fig. 7A), suggesting that the combination therapy effectively promoted the differentiation of OPC into immature OL to induce myelination.

Combination therapy promoted OPC differentiation by inhibiting PRKCD expression

To investigate the specific mechanism of the combined treatment in myelination, proteomic sequencing was employed to analyze the protein content in the motor cortex. High-throughput protein sequencing identified a total of 434 DEPs (fold change > 1.5, $p < 0.05$, Fig. 8A and Additional file 1). By intersecting the four groups of DEPs, we found eight co-expressed DEPs (RGD1566265, DEK, PRKCD, EDC4, CHMP2A, TCEAL5, ESYT1 and PTPRN2, Additional file 1). In addition, we searched the DrugBank database for drug targets associated with 'cerebral palsy', 'cerebral hypoxia-ischemia' and 'white matter injury', yielding a total of 102 drug targets (Additional file 1). When the CP drug targets were intersected with the co-expressed DEPs, PRKCD was identified as a key factor of the synergistic effects of combined therapy (Fig. 8B). Qualitative and quantitative analysis of PRKCD revealed that both protein and mRNA expression of PRKCD were significantly increased in the HCP group compared to the control group ($p < 0.01$, Fig. 8C-E). However, the protein and mRNA expression levels of PRKCD after CIMT + MSC and MSC interventions were significantly lower than those in the HCP group ($p < 0.05$, Fig. 8C-D). Notably, the protein expression of PRKCD was significantly lower in the CIMT + MSC group than in the CIMT group ($p < 0.05$, Fig. 8D), suggesting that the combined intervention could suppress the expression of PRKCD.

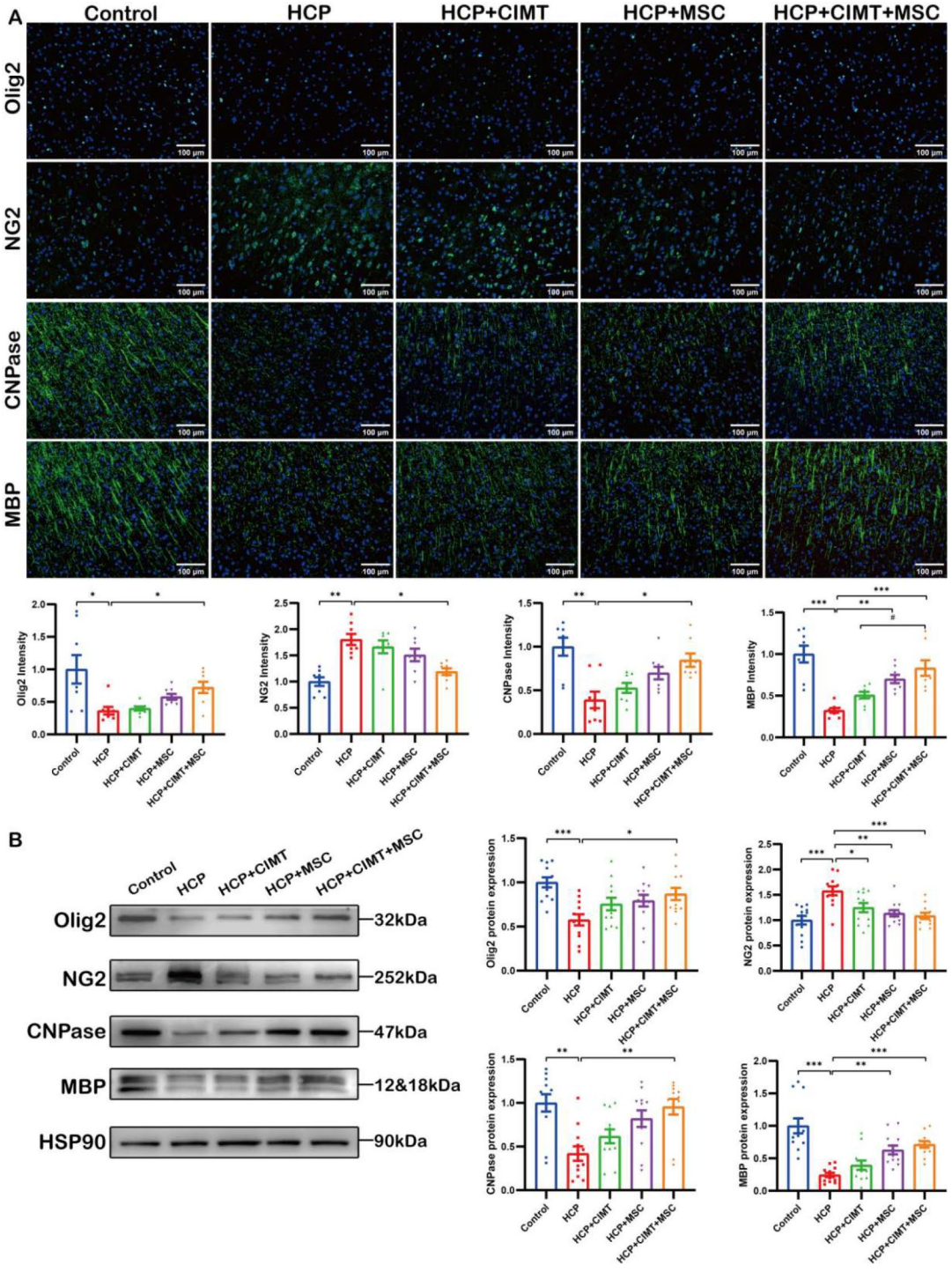

Fig. 6 Expression of oligodendrocyte-related proteins in the motor cortex. (**A**) Expression of Olig2, NG2, CNPase and MBP in the motor cortex in each group assessed by immunofluorescence staining ($n = 4*2$, 2 sections from each rat), scale bar = 100 μm; (**B**) Expressions of Olig2, NG2, CNPase and MBP analyzed with Western blotting in each group ($n = 4*3$, repeated three times per group). The data are shown as the mean ± SEM. HCP: hemiplegic cerebral palsy; CIMT: constraint-induced movement therapy; MSC: mesenchymal stem cell. Olig2: oligodendrocyte transcription factor 2; NG2: neuron-glial antigen 2; CNPase: 2′,3′-cyclic nucleotide 3′-phosphodiesterase; MBP: myelin basic protein. Full-length blots are presented in Additional file 2. (* $p < 0.05$, ** $p < 0.01$, *** $p < 0.001$ vs. HCP group; # $p < 0.05$ vs. HCP + CIMT + MSC group)

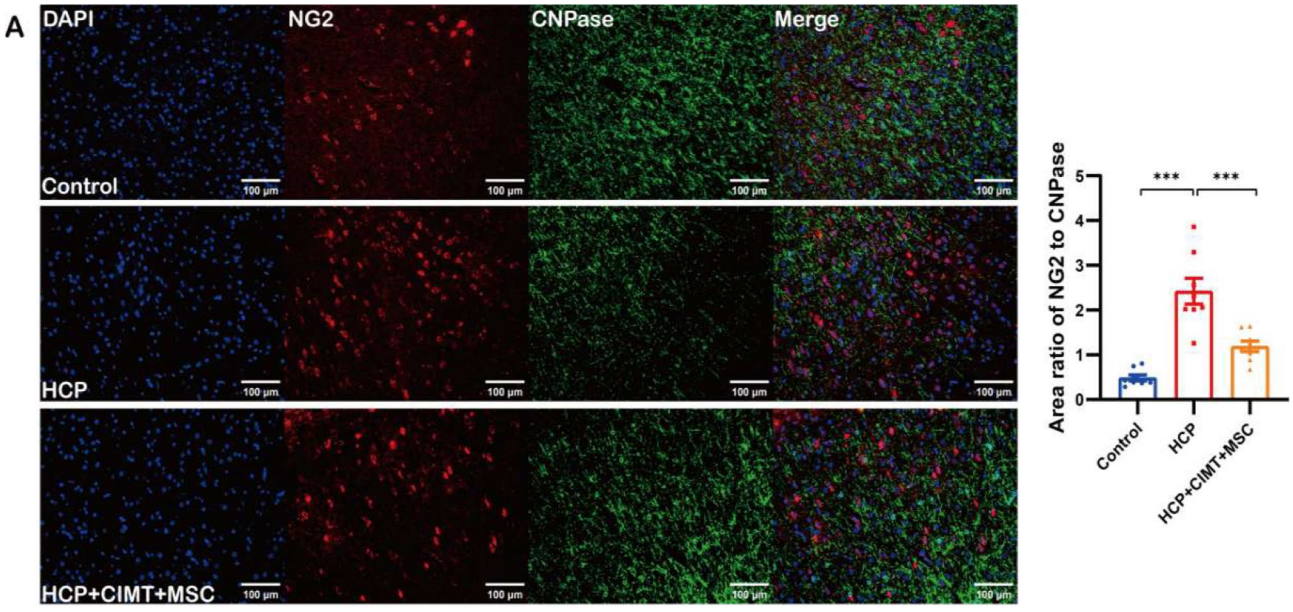

Fig. 7 Combined treatment promotes the differentiation of oligodendrocyte progenitors into immature oligodendrocytes. (**A**) Expressions of NG2 and CNPase positive cells assessed by immunofluorescence staining and ratio of fluorescence area of NG2 and CNPase positive cells in each group ($n = 4*2$, 2 sections from each rat), scale bar = 100 μm. The data are shown as the mean ± SEM. HCP: hemiplegic cerebral palsy; CIMT: constraint-induced movement therapy; MSC: mesenchymal stem cell. NG2: neuron-glial antigen 2; CNPase: 2',3'-cyclic nucleotide 3'-phosphodiesterase. (*** $p < 0.001$ vs. HCP group)

To further investigate the role of PRKCD in OL differentiation, we performed fluorescent co-localization of PRKCD with NG2, Olig2, CNPase, and MBP (Fig. 9A). The results showed co-expression of PRKCD with a large number of $NG2^+$ OPC, a smaller number of $Olig2^+$ OL and no co-expression with $CNPase^+$ OL or MBP^+ OL. This suggests that PRKCD is predominantly expressed in OPC and may regulate their physiological processes. We then observed that the number of $PRKCD^+/NG2^+$ OPC was higher and the $CNPase^+$ OL and $PRKCD^+$ area ratio was lower in the HCP group than in the control group ($p < 0.001$, Fig. 9B). However, combination therapy decreased $PRKCD^+/NG2^+$ OPCs but increased the $CNPase^+$ OL and $PRKCD^+$ area ratio ($p < 0.05$, Fig. 9B), indicating that co-intervention might facilitate the differentiation of OPC into immature OL by inhibiting PRKCD expression.

CIMT combined with hUC-MSCs transplantation promoted OPC differentiation through Inhibition of the MEK/ERK pathway

The mitogen activated protein kinase kinase (MEK)/extracellular signal regulated kinase (ERK) pathway is critical for regulating essential processes such as cell proliferation, differentiation, and survival [42]. In investigation of the KEGG pathways associated with PRKCD, we discovered that PRKCD could activate the MEK/ERK signaling, either directly or indirectly (KEGG PATHWAY Database: map04722). To assess whether CIMT combined with hUC-MSCs activates the MEK/ERK pathway in HCP rats, we performed western blot analysis to evaluate the levels of phosphorylated MEK1/2 (p-MEK1/2) and phosphorylated ERK1/2 (p-ERK1/2) (Fig. 10A). Our results showed that the levels of p-MEK1/2 and p-ERK1/2 were significantly higher in the HCP group compared to the control group ($p < 0.05$, respectively, Fig. 10B-C). However, after combined intervention, we observed significantly lower levels of p-MEK1/2 and p-ERK1/2 ($p < 0.05$, respectively, Fig. 10B-C). These findings suggested that CIMT combined with hUC-MSCs might facilitate OPC differentiation and myelination by inhibiting the activation of PRKCD/MEK/ERK signal pathway in HCP rats.

Discussion

In this study, we used a model of immature brain injury as delineated in a previous publication to recapitulate the brain injury observed in children with HCP [19]. We demonstrated that CIMT combined with intrathecal hUC-MSCs injection might synergistically promote the differentiation of OPC into immature OL and induce myelination by inhibiting the PRKCD/MEK/ERK signaling, and suggesting that myelin structural remodeling drove functional reorganization which substantially improved motor function in HCP rats. In addition to making it easier to guide the use of combination therapies from a clinically relevant experimental design, the study further proposed distinct insights into the mechanisms by which PRKCD/MEK/ERK mediates combination

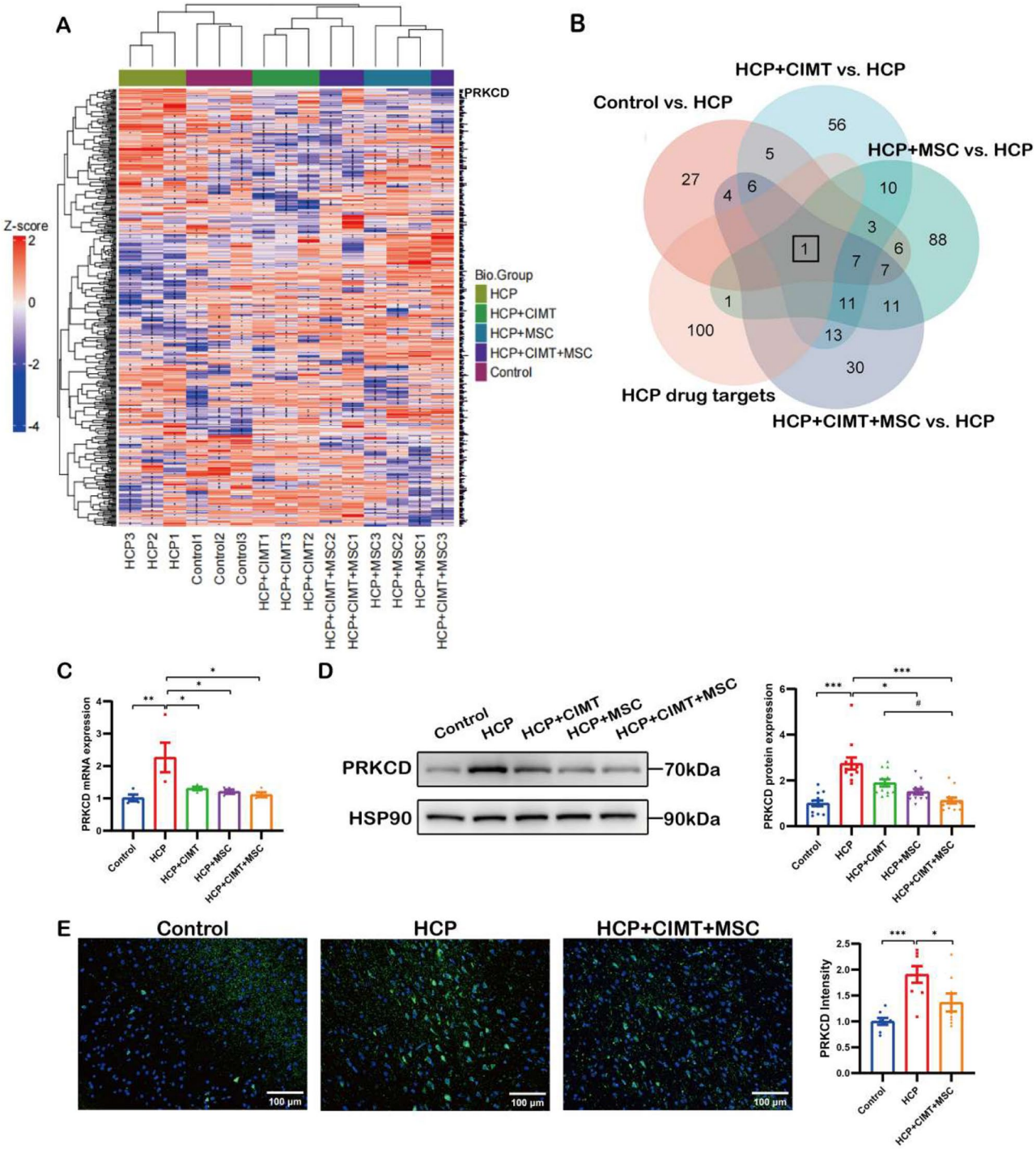

Fig. 8 Proteomics analysis after intervention and screening and validation of differential proteins. (**A**) Clustering heatmap of all significant proteins in each group; (**B**) Venn diagram of differential expressed proteins in each group and cerebral palsy drug targets; (**C**) Comparison of the mRNA expression of PRKCD among the groups ($n=4$); (**D**) Comparison of the expression of PRKCD analyzed by Western blotting among the groups ($n=4*3$, repeated three times per group); (**E**) Comparison of the expression of PRKCD in the motor cortex assessed by immunofluorescence staining among the groups ($n=4*2$, 2 sections from each rat), scale bar = 100 μm. The data are shown as the mean ± SEM. HCP: hemiplegic cerebral palsy; CIMT: constraint-induced movement therapy; MSC: mesenchymal stem cell; PRKCD: protein kinase C delta. Full-length blots are presented in Additional file 2. (* $p<0.05$, ** $p<0.01$, *** $p<0.001$ vs. HCP group; # $p<0.05$ vs. HCP + CIMT + MSC group)

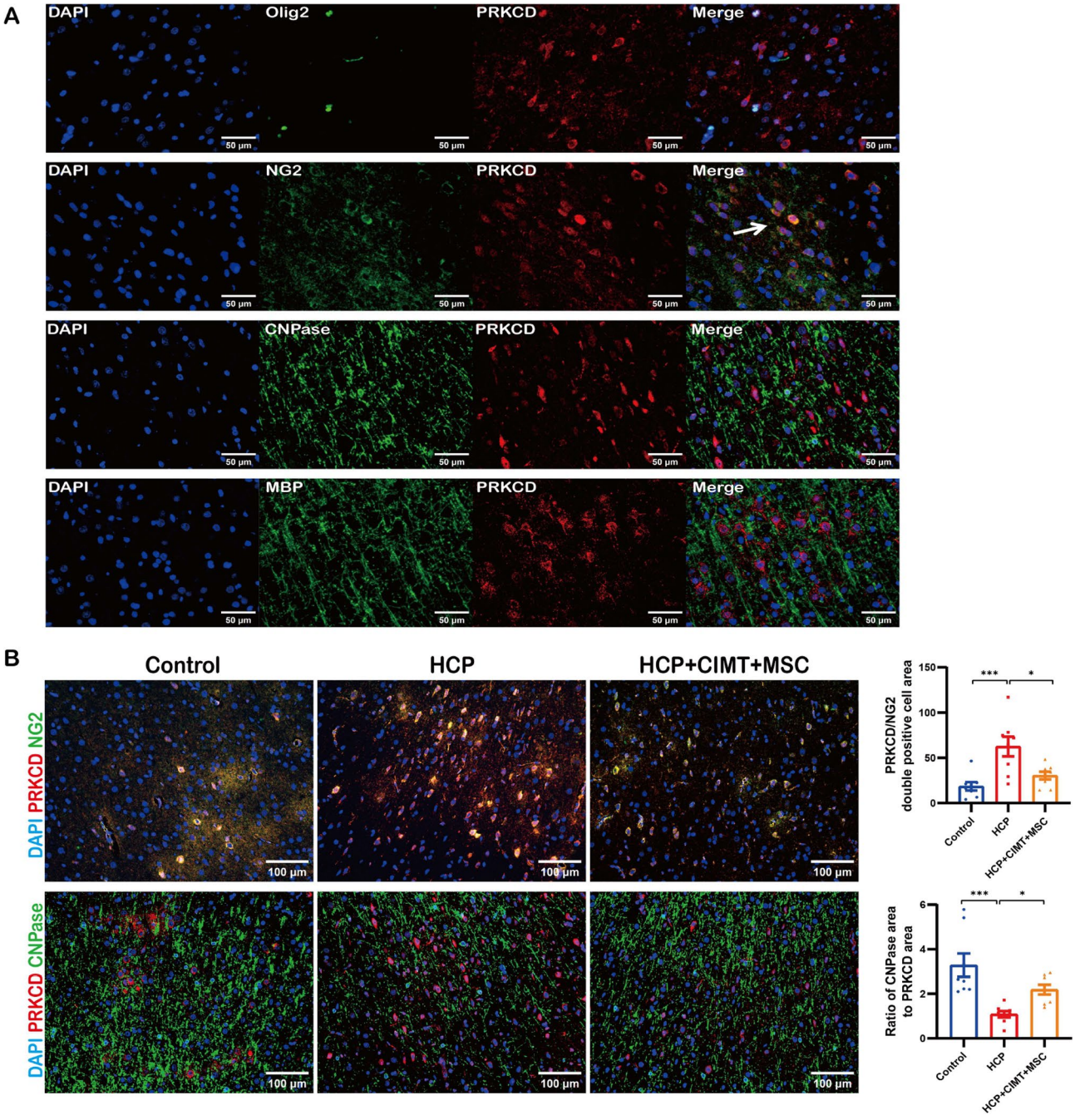

Fig. 9 Combination therapy promotes OPC differentiation by inhibiting PRKCD expression. (**A**) Fluorescence co-localization of PRKCD with NG2, Olig2, CNPase, and MBP, scale bar = 50 μm; (**B**) Comparison of the area of PRKCD/NG2 double positive cells and ratio of fluorescence area of CNPase/PRKCD positive cells in each group ($n = 4*2$, 2 sections from each rat), scale bar = 100 μm. The data are shown as the mean ± SEM. HCP: hemiplegic cerebral palsy; CIMT: constraint-induced movement therapy; MSC: mesenchymal stem cell; Olig2: oligodendrocyte transcription factor 2; NG2: neuron-glial antigen 2; CNPase: 2',3'-cyclic nucleotide 3'-phosphodiesterase; MBP: myelin basic protein; PRKCD: protein kinase C delta. (* $p < 0.05$, *** $p < 0.001$ vs. HCP group)

therapy-related neurobehavior from the viewpoint of myelination.

Brain injury in HCP is predominantly characterized by white matter damage, persistent myelin defects, and reduced plasticity, usually accompanied by a decrease in myelinated OL [25, 43, 44]. Optimizing motor cortical circuits, promoting differentiation of OL, and inducing myelination may hold the key to improving HCP brain injury [45, 46]. We have established an HCP model using 5-day-old rat pups to mimic 32-36-week-old human immature brains, as the white matter vulnerability of rodents at this time [47]. OPC is more sensitive to

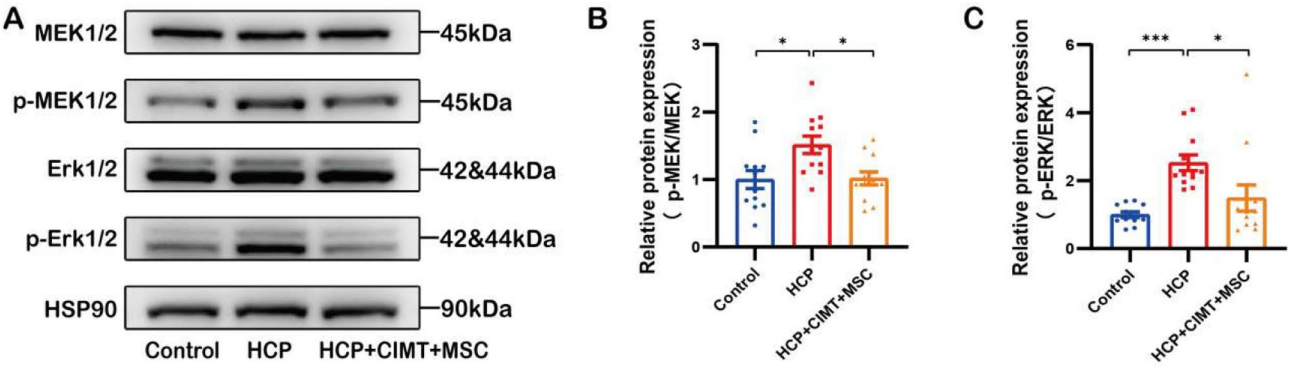

Fig. 10 Combination therapy inhibits MEK/ERK pathway activation. (**A**) Expressions of MEK1/2 and ERK1/2 total protein and phosphorylated protein analyzed by Western blotting in each group; (**B**) Comparison of the protein expression of p-MEK1/2 phosphorylated protein among the groups ($n=4*3$, repeated three times per group); (**C**) Comparison of the protein expression of p-ERK1/2 phosphorylated protein among the groups ($n=4*3$, repeated three times per group). The data are shown as the mean ± SEM. HCP: hemiplegic cerebral palsy; CIMT: constraint-induced movement therapy; MSC: mesenchymal stem cell; PRKCD: protein kinase C delta; MEK: mitogen-activated protein kinase kinase; ERK: extracellular regulated kinase; p-MEK: phospho-MEK; p-ERK: phospho-ERK. Full-length blots are presented in Additional file 2. (* $p<0.05$, *** $p<0.001$ vs. HCP group)

HI-induced injury at this stage, as evidenced by a multifold expansion of the OPC pool, a persistent maturation arrest and impaired differentiation into myelin-producing cells [43, 45]. At 24 h post-operation, the cerebral infarction area reached 20–30% of total brain volume. By P18, the left motor cortex showed approximately 50% neuronal loss accompanied by significant tissue atrophy, correlating with 50% impairment in motor function. Until P49, motor deficits persisted at 40% of normal levels with significant myelin disruption. This series of findings demonstrates persistent hypoxic-ischemic injury across developmental stages. Subsequently, rats at P20-21 were selected for CIMT and hUC-MSCs transplantation, mimicking the clinical treatment timeline for 2-3-year-old children diagnosed with HCP [47, 48].

Due to no cure currently exists for HCP, rehabilitation such as CIMT are mainly used in clinical practice though their efficacy remains suboptimal [9, 10]. Stem cell transplantation, which directly targets potential brain injury to reduce the severity, is a promising etiological treatment for HCP [49]. However, as HCP is typically diagnosed between 12 and 24 months, stem cell transplantation often misses the narrow treatment window after brain injury [1]. Certain cellular therapies can re-stimulate plasticity mechanisms and promote rehabilitation-induced stabilization of newly formed neural circuits [26, 27]. Therefore, it is generally recommended to apply stem cell transplantation combined with rehabilitation strategies to achieve additional or synergistic therapeutic effects [50].

As adult stem cells, MSC has extensive accessibility, minimal tumorigenicity and significant paracrine effects in comparison to neural stem/precursor cells [51]. Allogeneic hUC-MSCs are less costly and time-consuming than the use of autologous bone marrow cells and is usually more suitable for children and adolescents [52]. Furthermore, MSCs possess low immunogenicity due to their lack of major histocompatibility complex class II (MHC-II) molecule expression [53]. Notably, human-derived MSCs have not been observed to induce significant immune rejection in rodent models, which provides substantial evidence supporting the safety of xenogeneic stem cell application in this study [19–21]. Compared to intracerebroventricular injections, intrathecal injections minimize tissue trauma, enable repeat injections, and are more suitable for clinical stem cell applications [12, 54, 55]. Our previous study indicated intrathecal injection of hUC-MSCs showed less trauma in HCP model, and the motor improvement could last at least 4 weeks after injection [19]. Therefore, we designed to conduct 2 weeks CIMT immediately after intrathecal hUC-MSCs transplantation and evaluation 2 weeks later, in order to observe the synergistic effects of combination therapy. Our results showed that combining CIMT with hUC-MSCs could achieve enhanced therapeutic outcomes on the motor function improvement when compared to monotherapies. In HCP rats, overall motor function and fatigue resistance showed a superimposed effect after combined treatment, whereas recovery of upper limb grip and endurance was secondary to the overall functional improvement. After intrathecal injection, hUC-MSCs were mainly localized in the cortex of the damaged side of the brain, peaking at 24 h after transplantation and gradually diminishing over time. During this period, CIMT was administered. The synergistic effect likely arises from transplanted stem cells surrounding the damaged cortex, enhancing CIMT-induced motor cortical circuit remodeling by secreting bioactive molecules that establish a favorable microenvironment [13, 27].

Functional recovery necessitates the formation of new neural connections and circuits, while remodeling of cortical neural circuits thrives on the integrity of myelin

[56–58]. Our results showed that both combination therapy and single CIMT or MSC treatment were effective in promoting myelination, which was consistent with previous studies [8, 19, 59]. In our study, the combination treatment increased dendritic spines and branches, suggesting enhanced neurogenesis and neuronal circuit recovery, although the change was not statistically significant compared to single treatment. At present, evidence from the HI model of immature brain injury [59] and the stroke model of mature brain injury [60, 61] has shown that the combined treatment can synergistically promote myelination and functional recovery after brain injury, which is in line with our findings. However, our experimental protocol, including stem cell type, injection timing, delivery route, and the restriction method of CIMT, closely resembles clinical interventions, facilitating translational applications.

Myelination after hypoxic-ischemic brain injury requires the involvement of oligodendrocyte lineage cells and relies on the generation of new mature OL by OPC [45, 62]. OPC migrate within tissues and extend multiple cell membrane processes to differentiate into OL, which eventually wrap around axons to form myelin sheaths [63]. Back noted that impaired white matter myelination was associated with abnormal OPC differentiation, which he attributed to the enlargement of OPC cell pools resulting from OPC plasticity responses in subacute lesions and the disruption of OPC differentiation into myelinated OL [43]. Biname et al. [64] and Gaesser et al. [65] expressed the same view, suggesting that promoting OPC differentiation may be a potential regenerative strategy for myelination in white matter lesions. Our study observed impaired OPC differentiation, with large numbers of OPC remaining 45 days after brain injury and a significant reduction in immature and mature OL. Combination therapy significantly reduced numbers of $NG2^+$ OPC and increased numbers of $Olig2^+$ OL, $CNPase^+$ OL, and MBP^+ OL, potentially linked to enhanced OPC differentiation. We then further confirmed by $NG2^+$/$CNPase^+$ fluorescence area analysis that combination therapy promoted OPC differentiation into immature OL induced myelin formation. The combined treatment strategy focusing on the normal differentiation process of OPC is proposed for the first time, which may make an essential contribution to long-term myelination in HCP. However, little was known about the role of combination therapy in OPC differentiation.

In the study, we identified a key factor of the synergistic effect of the combination therapy, PRKCD, which was expressed in OPC and involved in physiological process of OPC. PRKCD is a member of the novel calcium-independent protein kinase C (PKC) family and regulates cell proliferation, the cell cycle, and apoptosis, primarily through mediating the phosphorylation of target proteins [66]. MEK/ERK is a downstream signaling pathway of PRKCD in OL, regulating critical processes including cell proliferation, differentiation and survival [42, 67]. Studies have shown that ERK1/2 mediates early OPC differentiation and that inhibition of the MEK/ERK pathway promotes OL formation and recovery from demyelinating diseases [65, 68]. Pharmacological or siRNA-mediated inhibition of PKC signaling can induce OPC differentiation [69]. Therefore, we hypothesized that PRKCD/MEK/ERK pathway mediate the effects of CIMT combined with hUC-MSCs transplantation in promoting OPC differentiation in HCP rats. We then performed relevant experiments to verify this hypothesis. In the HCP group, both PRKCD protein and mRNA levels, as well as the number of $PRKCD^+/NG2^+$ double positive cells were significantly higher, along with increased phosphorylation levels of MEK and ERK. Following combination treatment, there was a more than 1-fold decrease in PRKCD protein and mRNA levels, as well as a reduction in PRKCD expression on NG2 glial cells. Additionally, MEK and ERK phosphorylation levels decreased by 0.5- to 1-fold, alongside an approximate 0.5-fold increase in CNPase and MBP levels. These results suggested that CIMT combined with hUC-MSCs improved HCP motor function, possibly by inhibiting the PRKCD/MEK/ERK pathway to promote the differentiation of OPC into OL, thereby inducing myelination.

Previous studies have shown that the effects of PKC on OPC and OL differ significantly, with activation of PKC in OPC appearing to be involved in increased proliferation and decreased differentiation, whereas activation of PKC in OL probably increases process extension and myelin formation [67]. Our results confirmed this distinction, demonstrating that PRKCD was specifically expressed on $NG2^+$ OPC and promoted OPC differentiation by inhibiting PRKCD activation. This may relate to Thr phosphorylation events within the cytoplasmic domain of the NG2 proteoglycan. ERK mediates the phosphorylation of NG2 at Thr^{2314}, stimulating cell proliferation [70, 71]. When combination therapy targeted the inhibition of PRKCD, it suppressed the activation of MEK and ERK, allowing OPC to exit the cell cycle and initiate a transcriptional programme to induce differentiation into mature OL [72, 73]. Our study supports an intrinsic mechanism by which PRKCD involves in OPC differentiation, and strategies that directly alter PRKCD activity or modulate PRKCD activation may be therapeutically useful. Therefore, the development of therapies targeting PRKCD and other PKC subtypes may have significant potential value in the treatment of diseases associated with defective myelination [69].

Limitations

There were several limitations to the present study. Firstly, the etiology of HCP is complex and varied, and our HI model cannot fully replicate brain injury in children with HCP. Secondly, in our study, we focused on the synergistic effect of the two therapies on myelination and did not explore other mechanism of the interaction between CIMT and hUC-MSCs. Further research is warranted to determine the complex interactions and the optimal timing and sequence of combination therapy. Thirdly, it is essential to characterize the signaling cascades during myelin regeneration. Finding only implied that combined interventions might promote the differentiation of OPC into immature OL by inhibiting the PRKCD/MEK/ERK signaling. The mechanism of interaction between PRKCD/ MEK/ERK pathways in OPC remains unclear, and the role of PRKCD/MEK/ERK in OPC differentiation and myelination requires further validation through cellular and animal experiments, as well as clinical verification in samples from individuals with upper limb palsy. Finally, although the current neurobehavioral assessments, myelin protein analyses, and neuronal morphology examinations provide valuable insights, these findings are insufficient to fully characterize neural circuit reorganization and functional remyelination. Future investigations should incorporate electrophysiological techniques to directly evaluate local and distal neural signal transmission, which would provide more comprehensive evidence of functional recovery.

Conclusions

CIMT combined with hUC-MSCs intrathecal transplantation synergistically promoted myelination and restored motor function in HCP rats. The mechanisms might be relevant to promote the differentiation of OPC into immature OL and induce myelination by inhibiting PRKCD/MEK/ERK signaling. These findings highlighted a synergistic effect of CIMT combined with hUC-MSCs, broadening the clinical treatment strategy for HCP and identifying a promising target for therapeutic intervention.

Abbreviations

CIMT	Constraint induced movement therapy
CNPase	2',3'-cyclic nucleotide 3'-phosphodiesterase
DAPI	49,69-diamidino-2-phenylindole dihy drochloride hydrate
ERK	Extracellular regulated kinase
HCP	Hemiplegic cerebral palsy
HI	Hypoxic-ischemic
hUC-MSCs	Human umbilical cord-derived mesenchymal stem cells
LC-MS	Liquid chromatography-mass spectrometry tandem technology
MBP	Myelin basic protein
MEK	Mitogen-activated protein kinase kinase
MSC	Mesenchymal stem cell
NG2	Neural-glial antigen 2
OL	Oligodendrocytes
Olig2	Oligodendrocyte transcription factor 2
OPC	Oligodendrocyte precursor cells
PRKCD	Protein kinase C delta
QPCR	Quantitative real-time polymerase chain reaction
TEM	Transmission electron microscopy
TTC	2, 3, 4-triphenyltetrazolium chloride

Supplementary Information

The online version contains supplementary material available at https://doi.org/10.1186/s13287-025-04544-7.

Supplementary Material 1

Acknowledgements

We would like to thank Shu Pu Biotechnologies LLC (Shanghai, China) for proteomics technical assistance.

Author contributions

Experimental design: Lu He, Kaishou Xu, Xiaolin Guo. Conducted experiments: Xiaolin Guo, Tingting Peng (Junior, 2001), You Wang. Performed data analysis: Xiaolin Guo, Mengru Zhong, Yage Zhang. Data statistics and interpretation: Shiya Huang, Xiaoli Zeng, Tingting Peng (Senior, 1996) and Aihua Chen. Wrote or contribution to the writing of the manuscript: Xiaolin Guo, Jie Luo, Liru Liu. Review and final approval of the manuscript: Lu He, Kaishou Xu. All authors read and approved the final manuscript.

Funding

The study was funded by the National Natural Science Foundation of China (82472598), Guangzhou Municipal Science and Technology Project (2024A03J01274), and the Featured Clinical Technique of Guangzhou (2023C-TS59).

Data availability

All original contributions presented in the study are included in the article/Supplementary Material. Further inquiries can be directed to the corresponding author. The authors did not use any generative artificial intelligence (AI) and AI-assisted technologies in the writing process of the manuscript.

Declarations

Ethics approval and consent to participate

All procedures were approved by the Laboratory Animal Committee of Guangzhou Women and Children's Medical Center. (1) Title of the approved project: Constraint-induced movement therapy combined with mesenchymal stem cell transplantation promotes myelination and functional recovery in hemiplegic cerebral palsy rats; (2) Name of the institutional approval committee: Laboratory Animal Committee of Guangzhou Women and Children's Medical Center; (3) Approval number: RSDW-2023-01402; (4) Date of approval: 13th December 2023. Human material has been performed in accordance with the Declaration of Helsinki. The hUC-MSCs used in this study were all supplied by Guangdong Xiangxue Stem Cell Regenerative Medicine Technology Co., Ltd, and approved by the National Institutes for Food and Drug Control (Report number: SH202207163, Date of approval: 4th November 2022). Human umbilical cord tissue was sourced from healthy volunteer pregnant women, all of whom signed an informed consent form prior to delivery.

Consent for publication

Not applicable.

Competing interests

The authors declare that they have no competing interests.

Author details

[1]Department of Rehabilitation, Guangzhou Women and Children's Medical Center, Guangzhou Medical University, Guangzhou 510120, China
[2]School of Exercise and Health, Shanghai University of Sport, Shanghai 200438, China

[3]Guangdong Xiangxue Stem Cell Regenerative Medicine Technology Co., Ltd, Guangzhou 510005, China

Received: 30 December 2024 / Accepted: 18 July 2025
Published online: 21 August 2025

References

1. Novak I, Morgan C, Adde L, Blackman J, Boyd RN, Brunstrom-Hernandez J, et al. Early, accurate diagnosis and early intervention in cerebral palsy: advances in diagnosis and treatment. JAMA Pediatr. 2017;171(9):897–907.
2. McIntyre S, Goldsmith S, Webb A, Ehlinger V, Hollung SJ, McConnell K, et al. Global prevalence of cerebral palsy: A systematic analysis. Dev Med Child Neurol. 2022;64(12):1494–506.
3. Cieza A, Causey K, Kamenov K, Hanson SW, Chatterji S, Vos T. Global estimates of the need for rehabilitation based on the global burden of disease study 2019: a systematic analysis for the global burden of disease study 2019. Lancet. 2021;396(10267):2006–17.
4. Novak I, Morgan C, Fahey M, Finch-Edmondson M, Galea C, Hines A, et al. State of the evidence traffic lights 2019: systematic review of interventions for preventing and treating children with cerebral palsy. Curr Neurol Neurosci Rep. 2020;20(2):3.
5. Zelnik N, Lahat E, Heyman E, Livne A, Schertz M, Sagie L, et al. The role of prematurity in patients with hemiplegic cerebral palsy. J Child Neurol. 2016;31(6):678–82.
6. Dionisio MC, Terrill AL. Constraint-Induced movement therapy for infants with or at risk for cerebral palsy: A scoping review. Am J Occup Ther. 2022;76(2).
7. Fu C, Tang H, Liu L, Huang Y, Zhou H, Huang S et al. Constraint-Induced movement therapy promotes Myelin remodeling and motor function by mediating Sox2/Fyn signals in rats with hemiplegic cerebral palsy. Phys Ther. 2024;104(5).
8. Liu LR, Wang YX, He L, Xu YX, Huang JY, Peng TT, et al. Constraint-Induced movement therapy promotes neural remodeling and functional reorganization by overcoming Nogo-A/NgR/RhoA/ROCK signals in hemiplegic cerebral palsy mice. Neurorehabil Neural Repair. 2021;35(2):145–57.
9. Hoare BJ, Wallen MA, Thorley MN, Jackman ML, Carey LM, Imms C. Constraint-induced movement therapy in children with unilateral cerebral palsy. Cochrane Database Syst Rev. 2019;4(4):Cd004149.
10. Yang FA, Lee TH, Huang SW, Liou TH, Escorpizo R, Chen HC. Upper limb manual training for children with cerebral palsy: A systematic review and network meta-analysis of randomized controlled trials. Clin Rehabil. 2023;37(4):516–33.
11. Lv ZY, Li Y, Liu J. Progress in clinical trials of stem cell therapy for cerebral palsy. Neural Regen Res. 2021;16(7):1377–82.
12. Qu J, Zhou L, Zhang H, Han D, Luo Y, Chen J, et al. Efficacy and safety of stem cell therapy in cerebral palsy: A systematic review and meta-analysis. Front Bioeng Biotechnol. 2022;10:1006845.
13. Sun JM, Kurtzberg J. Stem cell therapies in cerebral palsy and autism spectrum disorder. Dev Med Child Neurol. 2021;63(5):503–10.
14. Xie Q, Liu R, Jiang J, Peng J, Yang C, Zhang W, et al. What is the impact of human umbilical cord mesenchymal stem cell transplantation on clinical treatment? Stem Cell Res Ther. 2020;11(1):519.
15. Fong CY, Chak LL, Biswas A, Tan JH, Gauthaman K, Chan WK, et al. Human wharton's jelly stem cells have unique transcriptome profiles compared to human embryonic stem cells and other mesenchymal stem cells. Stem Cell Rev Rep. 2011;7(1):1–16.
16. Blanco-Elices C, Chato-Astrain J, González-González A, Sánchez-Porras D, Carriel V, Fernández-Valadés R et al. Histological profiling of the human umbilical cord: A potential alternative cell source in tissue engineering. J Pers Med. 2022;12(4).
17. Luo Y, Qu J, He Z, Zhang M, Zou Z, Li L, et al. Human umbilical cord mesenchymal stem cells improve the status of hypoxic/ischemic cerebral palsy rats by downregulating nogoa/ngr/rho pathway. Cell Transpl. 2023;32:9636897231210069.
18. Liau LL, Ruszymah BHI, Ng MH, Law JX. Characteristics and clinical applications of wharton's jelly-derived mesenchymal stromal cells. Curr Res Transl Med. 2020;68(1):5–16.
19. Huang S, Liu L, Huang Y, Fu C, Peng T, Yang X, et al. Potential optimized route for mesenchymal stem cell transplantation in a rat model of cerebral palsy. Exp Cell Res. 2023;430(2):113734.
20. Jiao Y, Sun YT, Chen NF, Zhou LN, Guan X, Wang JY, et al. Human umbilical cord-derived mesenchymal stem cells promote repair of neonatal brain injury caused by hypoxia/ischemia in rats. Neural Regen Res. 2022;17(11):2518–25.
21. Chen KH, Shao PL, Li YC, Chiang JY, Sung PH, Chien HW, et al. Human umbilical Cord-Derived mesenchymal stem cell therapy effectively protected the brain architecture and neurological function in rat after acute traumatic brain injury. Cell Transpl. 2020;29:963689720929313.
22. Ferre CL, Babik I, Michel GF. A perspective on the development of hemispheric specialization, infant handedness, and cerebral palsy. Cortex. 2020;127:208–20.
23. Scheck SM, Fripp J, Reid L, Pannek K, Fiori S, Boyd RN, et al. Extent of altered white matter in unilateral and bilateral periventricular white matter lesions in children with unilateral cerebral palsy. Res Dev Disabil. 2016;55:368–76.
24. Kirton A, Metzler MJ, Craig BT, Hilderley A, Dunbar M, Giuffre A, et al. Perinatal stroke: mapping and modulating developmental plasticity. Nat Rev Neurol. 2021;17(7):415–32.
25. Kuczynski AM, Dukelow SP, Hodge JA, Carlson HL, Lebel C, Semrau JA, et al. Corticospinal tract diffusion properties and robotic visually guided reaching in children with hemiparetic cerebral palsy. Hum Brain Mapp. 2018;39(3):1130–44.
26. Berlet R, Anthony S, Brooks B, Wang ZJ, Sadanandan N, Shear A et al. Combination of stem cells and rehabilitation therapies for ischemic stroke. Biomolecules. 2021;11(9).
27. Ito A, Kubo N, Liang N, Aoyama T, Kuroki H. Regenerative rehabilitation for stroke recovery by inducing synergistic effects of cell therapy and neurorehabilitation on motor function: A narrative review of Pre-Clinical studies. Int J Mol Sci. 2020;21(9).
28. National RC. Guide for the Care and Use of Laboratory Animals, 8th edition. Washington (DC): National Academies Press; 2011.
29. Festing MF. On determining sample size in experiments involving laboratory animals. Lab Anim. 2018;52(4):341–50.
30. Ismail TR, Yap CG, Naidu R, Pamidi N. Enrichment protocol for rat models. Curr Protoc. 2021;1(6):e152.
31. Rahman MM, Lee JY, Kim YH, Park CK. Epidural and intrathecal drug delivery in rats and mice for experimental research: fundamental concepts, techniques, precaution, and application. Biomedicines. 2023;11(5).
32. Ward JM, Rehg JE. Rodent immunohistochemistry: pitfalls and troubleshooting. Vet Pathol. 2014;51(1):88–101.
33. Ishiuchi N, Nakashima A, Maeda S, Miura Y, Miyasako K, Sasaki K, et al. Comparison of therapeutic effects of mesenchymal stem cells derived from superficial and deep subcutaneous adipose tissues. Stem Cell Res Ther. 2023;14(1):121.
34. Paxinos G, Watson C. The rat brain in stereotaxic Coordinates-7th edition. New York: Academic; 2013.
35. Liu F, Schafer DP, McCullough LD. TTC, fluoro-Jade B and NeuN staining confirm evolving phases of infarction induced by middle cerebral artery occlusion. J Neurosci Methods. 2009;179(1):1–8.
36. Du F. Golgi-Cox staining of neuronal dendrites and dendritic spines with FD rapid golgistain™ kit. Curr Protoc Neurosci. 2019;88(1):e69.
37. Tizro P, Choi C, Khanlou N. Sample Preparation for transmission electron microscopy. Methods Mol Biol. 2019;1897:417–24.
38. Pillai-Kastoori L, Schutz-Geschwender AR, Harford JA. A systematic approach to quantitative Western blot analysis. Anal Biochem. 2020;593:113608.
39. Im K, Mareninov S, Diaz MFP, Yong WH. An introduction to performing Immunofluorescence staining. Methods Mol Biol. 2019;1897:299–311.
40. Taylor SC, Nadeau K, Abbasi M, Lachance C, Nguyen M, Fenrich J. The ultimate qPCR experiment: producing publication quality, reproducible data the first time. Trends Biotechnol. 2019;37(7):761–74.
41. Huang Y, Chen Z, Xu Y, Liu L, Tang H, He L, et al. Proteomic changes of the bilateral M1 and spinal cord in hemiplegic cerebral palsy mouse: effects of constraint-induced movement therapy. Behav Brain Res. 2023;452:114583.
42. Wen X, Jiao L, Tan H. MAPK/ERK pathway as a central regulator in vertebrate organ regeneration. Int J Mol Sci. 2022;23(3).
43. Back SA. White matter injury in the preterm infant: pathology and mechanisms. Acta Neuropathol. 2017;134(3):331–49.
44. Baker K, Carlson HL, Zewdie E, Kirton A. Developmental remodelling of the motor cortex in hemiparetic children with perinatal stroke. Pediatr Neurol. 2020;112:34–43.
45. Motavaf M, Piao X. Oligodendrocyte development and implication in perinatal white matter injury. Front Cell Neurosci. 2021;15:764486.

46. Niu J, Yu G, Wang X, Xia W, Wang Y, Hoi KK et al. Oligodendroglial ring finger protein Rnf43 is an essential injury-specific regulator of oligodendrocyte maturation. Neuron. 2021;109(19):3104-18.e6.
47. Semple BD, Blomgren K, Gimlin K, Ferriero DM, Noble-Haeusslein LJ. Brain development in rodents and humans: identifying benchmarks of maturation and vulnerability to injury across species. Prog Neurobiol. 2013;106–107:1–16.
48. Morgan C, Fetters L, Adde L, Badawi N, Bancale A, Boyd RN, et al. Early intervention for children aged 0 to 2 years with or at high risk of cerebral palsy: international clinical practice guideline based on systematic reviews. JAMA Pediatr. 2021;175(8):846–58.
49. Xiao QX, Geng MJ, Sun YF, Pi Y, Xiong LL. Stem cell therapy in neonatal Hypoxic-Ischemic encephalopathy and cerebral palsy: a bibliometric analysis and new strategy. Mol Neurobiol. 2024;61(7):4538–64.
50. Boltze J, Modo MM, Mays RW, Taguchi A, Jolkkonen J, Savitz SI. Stem cells as an emerging paradigm in stroke 4: advancing and accelerating preclinical research. Stroke. 2019;50(11):3299–306.
51. Li YQ, Li PF, Tao Q, Abuqeis IJA, Xiyang YB. Role and limitation of cell therapy in treating neurological diseases. Ibrain. 2024;10(1):93–105.
52. Wang X, Hu H, Hua R, Yang J, Zheng P, Niu X, et al. Effect of umbilical cord mesenchymal stromal cells on motor functions of identical twins with cerebral palsy: pilot study on the correlation of efficacy and hereditary factors. Cytotherapy. 2015;17(2):224–31.
53. Wu X, Jiang J, Gu Z, Zhang J, Chen Y, Liu X. Mesenchymal stromal cell therapies: Immunomodulatory properties and clinical progress. Stem Cell Res Ther. 2020;11(1):345.
54. Kawabori M, Tanimori A, Kitta S, Shichinohe H, Houkin K. Evaluation of novel stereotactic cannula for stem cell transplantation against central nervous system disease. Stem Cells Int. 2020;2020:4085617.
55. Kim H, Na DL, Lee NK, Kim AR, Lee S, Jang H. Intrathecal Injection in A Rat Model: A Potential Route to Deliver Human Wharton's Jelly-Derived Mesenchymal Stem Cells into the Brain. Int J Mol Sci. 2020;21(4).
56. Almeida RG, Lyons DA. On myelinated axon plasticity and neuronal circuit formation and function. J Neurosci. 2017;37(42):10023–34.
57. Bonetto G, Belin D, Káradóttir RT, Myelin. A gatekeeper of activity-dependent circuit plasticity? Science. 2021;374(6569):eaba6905.
58. de Faria O Jr., Pivonkova H, Varga B, Timmler S, Evans KA, Káradóttir RT. Periods of synchronized Myelin changes shape brain function and plasticity. Nat Neurosci. 2021;24(11):1508–21.
59. Rumajogee P, Altamentova S, Li J, Puvanenthirarajah N, Wang J, Asgarihafshejani A et al. Constraint-Induced movement therapy (CIMT) and neural precursor cell (NPC) transplantation synergistically promote anatomical and functional recovery in a Hypoxic-Ischemic mouse model. Int J Mol Sci. 2024;25(17).
60. Jiang XH, Li HF, Chen ML, Zhang YX, Chen HB, Chen RH, et al. Treadmill exercise exerts a synergistic effect with bone marrow mesenchymal stem cell-derived exosomes on neuronal apoptosis and synaptic-axonal remodeling. Neural Regen Res. 2023;18(6):1293–9.
61. Yabuno S, Yasuhara T, Nagase T, Kawauchi S, Sugahara C, Okazaki Y, et al. Synergistic therapeutic effects of intracerebral transplantation of human modified bone marrow-derived stromal cells (SB623) and voluntary exercise with running wheel in a rat model of ischemic stroke. Stem Cell Res Ther. 2023;14(1):10.
62. Guillot M, Miller SP. The dimensions of white matter injury in preterm neonates. Semin Perinatol. 2021;45(7):151469.
63. Domingues HS, Cruz A, Chan JR, Relvas JB, Rubinstein B, Pinto IM. Mechanical plasticity during oligodendrocyte differentiation and myelination. Glia. 2018;66(1):5–14.
64. Binamé F, Pham-Van LD, Bagnard D. Manipulating oligodendrocyte intrinsic regeneration mechanism to promote remyelination. Cell Mol Life Sci. 2021;78(13):5257–73.
65. Gaesser JM, Fyffe-Maricich SL. Intracellular signaling pathway regulation of myelination and remyelination in the CNS. Exp Neurol. 2016;283(Pt B):501–11.
66. Reyland ME, Jones DN. Multifunctional roles of PKCδ: opportunities for targeted therapy in human disease. Pharmacol Ther. 2016;165:1–13.
67. Stariha RL, Kim SU. Protein kinase C and mitogen-activated protein kinase signalling in oligodendrocytes. Microsc Res Tech. 2001;52(6):680–8.
68. Suo N, Guo YE, He B, Gu H, Xie X. Inhibition of MAPK/ERK pathway promotes oligodendrocytes generation and recovery of demyelinating diseases. Glia. 2019;67(7):1320–32.
69. Baer AS, Syed YA, Kang SU, Mitteregger D, Vig R, Ffrench-Constant C, et al. Myelin-mediated Inhibition of oligodendrocyte precursor differentiation can be overcome by Pharmacological modulation of Fyn-RhoA and protein kinase C signalling. Brain. 2009;132(Pt 2):465–81.
70. Bottero M, Pessina G, Bason C, Vigo T, Uccelli A, Ferrara G. Nerve-Glial antigen 2: unmasking the enigmatic cellular identity in the central nervous system. Front Immunol. 2024;15:1393842.
71. Makagiansar IT, Williams S, Mustelin T, Stallcup WB. Differential phosphorylation of NG2 proteoglycan by ERK and PKCalpha helps balance cell proliferation and migration. J Cell Biol. 2007;178(1):155–65.
72. Mueller M, Oppliger B, Joerger-Messerli M, Reinhart U, Barnea E, Paidas M, et al. Wharton's jelly mesenchymal stem cells protect the immature brain in rats and modulate cell fate. Stem Cells Dev. 2017;26(4):239–48.
73. Damiano S, La Rosa G, Sozio C, Cavaliere G, Trinchese G, Raia M et al. 5-Hydroxytryptamine modulates maturation and mitochondria function of human oligodendrocyte progenitor M03-13 cells. Int J Mol Sci. 2021;22(5).

Publisher's note

Terms and Conditions

Springer Nature journal content, brought to you courtesy of Springer Nature Customer Service Center GmbH (“Springer Nature”).
Springer Nature supports a reasonable amount of sharing of research papers by authors, subscribers and authorised users (“Users”), for small-scale personal, non-commercial use provided that all copyright, trade and service marks and other proprietary notices are maintained. By accessing, sharing, receiving or otherwise using the Springer Nature journal content you agree to these terms of use (“Terms”). For these purposes, Springer Nature considers academic use (by researchers and students) to be non-commercial.
These Terms are supplementary and will apply in addition to any applicable website terms and conditions, a relevant site licence or a personal subscription. These Terms will prevail over any conflict or ambiguity with regards to the relevant terms, a site licence or a personal subscription (to the extent of the conflict or ambiguity only). For Creative Commons-licensed articles, the terms of the Creative Commons license used will apply.
We collect and use personal data to provide access to the Springer Nature journal content. We may also use these personal data internally within ResearchGate and Springer Nature and as agreed share it, in an anonymised way, for purposes of tracking, analysis and reporting. We will not otherwise disclose your personal data outside the ResearchGate or the Springer Nature group of companies unless we have your permission as detailed in the Privacy Policy.
While Users may use the Springer Nature journal content for small scale, personal non-commercial use, it is important to note that Users may not:

1. use such content for the purpose of providing other users with access on a regular or large scale basis or as a means to circumvent access control;
2. use such content where to do so would be considered a criminal or statutory offence in any jurisdiction, or gives rise to civil liability, or is otherwise unlawful;
3. falsely or misleadingly imply or suggest endorsement, approval , sponsorship, or association unless explicitly agreed to by Springer Nature in writing;
4. use bots or other automated methods to access the content or redirect messages
5. override any security feature or exclusionary protocol; or
6. share the content in order to create substitute for Springer Nature products or services or a systematic database of Springer Nature journal content.

In line with the restriction against commercial use, Springer Nature does not permit the creation of a product or service that creates revenue, royalties, rent or income from our content or its inclusion as part of a paid for service or for other commercial gain. Springer Nature journal content cannot be used for inter-library loans and librarians may not upload Springer Nature journal content on a large scale into their, or any other, institutional repository.
These terms of use are reviewed regularly and may be amended at any time. Springer Nature is not obligated to publish any information or content on this website and may remove it or features or functionality at our sole discretion, at any time with or without notice. Springer Nature may revoke this licence to you at any time and remove access to any copies of the Springer Nature journal content which have been saved.
To the fullest extent permitted by law, Springer Nature makes no warranties, representations or guarantees to Users, either express or implied with respect to the Springer nature journal content and all parties disclaim and waive any implied warranties or warranties imposed by law, including merchantability or fitness for any particular purpose.
Please note that these rights do not automatically extend to content, data or other material published by Springer Nature that may be licensed from third parties.
If you would like to use or distribute our Springer Nature journal content to a wider audience or on a regular basis or in any other manner not expressly permitted by these Terms, please contact Springer Nature at

onlineservice@springernature.com